Journal of Materials Chemistry A

REVIEW

View Article Online
View Journal | View Issue

Cite this: J. Mater. Chem. A, 2023, 11, 3262

Semiconductor quantum dots: a versatile platform for photoredox organic transformation

Hui-Li Wu, Ming-Yu Qi, Zi-Rong Tang * and Yi-Jun Xu *

Received 4th December 2022
Accepted 14th January 2023

DOI: 10.1039/d2ta09423a

rsc.li/materials-a

Semiconductor quantum dots (QDs), as a newfashioned light-absorbing material with great promise in artificial photosystems, generally exhibit attractive photoactivity and selectivity in organic photoredox transformation thanks to their tunable redox potential, high-efficiency light harvesting capability, and high extinction coefficient in the visible region. Utilizing QDs as a versatile platform to convert organic compounds into value-added feedstocks provides an effective way to alleviate energy and chemical feedstock supply problems. In this review, we concisely summarize the basic principles of photocatalytic organic conversions over semiconductor QDs and the effects of grain size, surface active sites and ligands on their catalytic performance. Then, we highlight the recent progress of QDs enabling multifarious photocatalytic organic transformations, including nitroaromatic reduction, selective alcohol oxidation, sulfide oxidation, C–H functionalization and so on. In the end, we discuss the current challenges and future prospects in further developing efficient semiconductor QD-based photocatalysts toward photoredox-catalyzed organic conversion.

1. Introduction

Organic synthesis chemistry plays a vital role in the manufacture of bulk commodities and other fine chemicals, which permeates people's daily life from chemical industry.[1] Nevertheless, the traditional organic synthesis is typically accompanied by the use of toxic or corrosive chemical reagents, which have caused severe damage to the environment.[2,3] For example, traditional industrial production commonly uses strong acids or bases to synthesize important organic chemicals at high temperature and pressure. The complex synthesis routes and harsh operating conditions also limit the sustainable development of traditional organic synthesis methods.[3,4] By contrast, the introduction of clean and renewable solar energy into organic synthesis reaction systems promotes the rapid development of photocatalytic organic conversion, which is undoubtedly an environmentally friendly and promising alternative.[5,6]

Among a variety of common photocatalysts, metal complexes (*e.g.*, [Ru], [Rh] and [Ir]) and bulk semiconductors (*e.g.*, TiO_2, ZnO and g-C_3N_4) are not ideal light absorbers for driving organic transformation due to the limited photostability of molecular species or the narrow absorption range of wide-bandgap materials.[7–9] In particular, some precious metal-based photocatalysts, such as polypyridyl complexes of Ru(II), Ir(III), and Pt(II), are not well suited for industrial productions on a large scale due to their limited practicability and high-energy consumption.[10] In comparison with other traditional semiconductor materials, semiconductor quantum dots (QDs) have become one of the most promising candidate materials in artificial photosystems by virtue of their wide absorption range, high extinction coefficient, effective charge transfer and stable photoactivity, providing a new versatile platform for photocatalytic organic synthesis.[10] By adjusting the structure (size or shape) or elemental composition of QDs, the redox potential of QDs, that is the bandgap, can be customized for diverse photocatalytic reactions. Besides, QDs can not only achieve surface functionalization through various organic or inorganic ligands without modifying the spectral absorption range or the redox potentials of the QDs, but also construct multifunctional heterostructure composites by surface assembly with other co-catalysts and/or other semiconductor photocatalysts, thus effectively regulating the photocatalytic performance for organic synthesis.[11,12] In addition, The colloidal properties of QD catalysts are conducive to the sufficient contact between catalysts and substrates and promotes the transfer of charge and energy, exhibiting the advantages of both homogeneous and heterogeneous catalysts.[10,13,14] The use of QD photocatalysts for organic transformation has been increasingly studied in recent years, because it opens up new and efficient pathways to synthesize high-value-added chemicals. Accordingly, it is highly desirable to afford an overview and detailed classifications of current advances on a QD-based composite system for selective photocatalytic organic synthesis.

Herein, we present a timely review to recap the recent progress of semiconductor QD-based catalysts in various

College of Chemistry, State Key Laboratory of Photocatalysis on Energy and Environment, Fuzhou University, Fuzhou 350116, China. E-mail: zrtang@fzu.edu.cn; yjxu@fzu.edu.cn

photoredox organic transfoxrmations. First, we clarify the fundamental principles of photocatalytic organic transformation over QD-based catalysts. In this part, the exciton generation, the formation of radical species and the influence of surface-chemistry-modification on selective organic conversion will be summarized. Later, we focus on the application of QD-based catalysts in photoredox organic transformations of various useful chemicals, which include nitroaromatic reduction, selective alcohol oxidation, C–H functionalization, sulfide oxidation, biomass valorization, *etc.* Finally, we will discuss the perspectives and possible challenges in photoredox-catalyzed organic transformation with QD-based catalysts.

2. Basic principles of photocatalytic organic synthesis of QD-based catalysts

2.1 The generation of charge carriers

The photocatalytic redox process starts with the generation of electron–hole pairs (charge carriers). Generally, after stimulation of QD-based catalysts by solar energy, electrons and holes can be simultaneously generated. On the one hand, the photoexcited electrons can readily be transferred to the conduction band (CB) for reduction reactions. On the other hand, the photogenerated holes left in the initial valence band (VB) can be used for oxidation reactions. Ideally, these photoexcited charge carriers generated in the bulk phase will migrate to the reactive sites on the surface to take part in the redox reactions.[15,16]

Typically, unlike bulk semiconductors (*e.g.*, TiO_2, WO_3, and g-C_3N_4) where a single incident photon produces only one exciton pair (electron–hole pair), semiconductor QDs exhibit unique properties in exciton generation due to quantum confinement effects.[17,18] For example, as shown in Fig. 1a, semiconductor QDs (especially PbTe, PbSe and PbS) are capable of generating multiple excitons after the absorption of one high-energy photon ($h\nu > 2E_g$).[19–21] When excited by an absorbed photon having energy more than twice their bandgap, semiconductor QDs may generate a pair of high-energy excitons, in which the energetic electron in the CB releases partial energy through impact ionization and falls back to the bottom of the CB, thus generating more new excitons and achieving efficient carrier multiplication to improve photocatalytic performance.[22–26] However, most single phase QDs have plenty of defects on the surface and a fast recombination rate of charge carriers, which is not favorable for improving the overall photocatalytic efficiency.[27] Moreover, the colloidal QDs have a very large specific surface area and many surface dangling bonds, some of which will introduce a large number of trap states, thus strongly localizing the photoexcited carriers and preventing them from further taking part in surface chemical reactions.[28] To overcome the above problems, a number of strategies have been explored for constructing efficient QD-based composite photocatalysts, which can better inhibit photogenerated charge carrier recombination and promote more rapid charge separation/transfer (Fig. 1b), such as combination with other

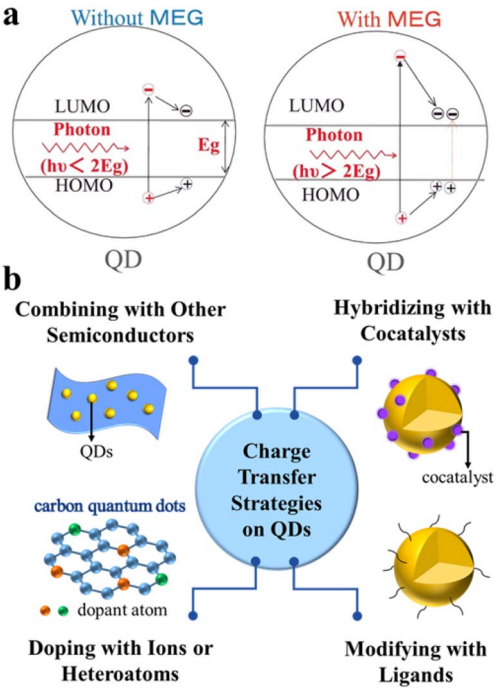

Fig. 1 (a) Schematic diagram of multiple exciton generation (MEG). Reprinted with permission from ref. 17. (b) Scheme of typical charge transfer strategies for QD catalysts.

matched semiconductors, doping with anions and/or cations or other heteroatoms, hybridization with suitable cocatalysts, and modification with inorganic/organic ligands.[29–33] Specifically, composite semiconductors, modified ligands, and loaded ions or atoms can all act as transporters of electrons or holes, and the construction of heterostructures inhibits photogenerated carrier recombination and prolongs the excited-state lifetime, thus achieving efficient selective organic conversion.

2.2 The formation of radicals

During photocatalytic organic conversion, the highly energetic charge carriers migrating from the catalyst phase to the surface are transferred to organic substrates or the solvent environment to induce the formation of reactive radicals, hence boosting the performance of the photocatalytic system. Fig. 2 summarizes the source and generation pathways of radicals in the organic transformation reaction system. Ideally, organic substrates can be directly activated by photoexcited catalysts *via* charge or energy transfer to form corresponsive radical intermediates which will further react to obtain target products with high selectivity.[34–37] For example, the C–H bond of benzyl alcohol is oxidized to form a $^{\bullet}$CH(OH)Ph radical by the photogenerated holes in the VB of CdS QDs after illumination. The unstable $^{\bullet}$CH(OH)Ph radical which is strongly adsorbed on the bare CdS QD surface can be further oxidized by the holes to produce benzaldehyde. However, over the CdS QDs anchored onto TiO_2 nanosheets, such a radical intermediate is directly coupled to form C–C products with high selectivity thanks to the effective transfer and accumulation of multiple electrons in the CdS/TNS

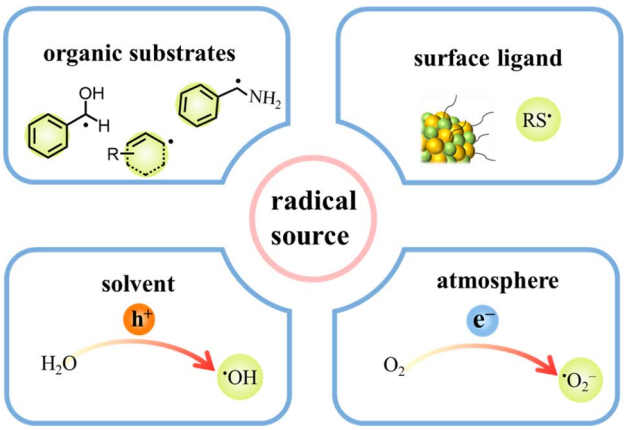

Fig. 2 Illustration of radical sources in the photocatalytic reaction system.

heterostructure.[38] Additionally, the surface ligands of QDs can also generate radicals, which will come into contact with organic substrates to initiate redox reactions.[39] For instance, the thiolate ligand attached to CdSe QDs generates a thiyl radical which extracts the hydrogen atom from the C–H bond of benzyl alcohol to produce a benzylic radical. Then, the benzylic radical induced by the thiyl radical is disproportionated to benzyl alcohol and benzaldehyde.[29] Furthermore, some radicals are derived from the gas atmosphere or solution environment, promoting the photocatalytic reaction indirectly as the active species (Fig. 2). On one hand, solvent molecules in the liquid phase can be activated to form radicals, such as water molecules losing electrons to generate hydroxyl radicals ($^{\bullet}OH$). On the other hand, O_2 can be dissolved in the reaction solvent and is more likely to capture electrons than H^+, generating superoxide radicals ($^{\bullet}O_2^-$) readily in the catalytic systems with an O_2 atmosphere.[40,41]

Some radical intermediates can be dynamically adsorbed on the surface of QDs, and go through a radical mediated reaction pathway to form a C–C/C–X bond (X = S, N, O).[37,42] Heterogeneous photocatalysis based on semiconductor QDs is a promising alternative approach for triggering radical coupling reactions in C–C/C–X bond synthesis, which has emerged as a hot direction in the photocatalysis research field because of its excellent efficiency and convenience in generating a variety of highly reactive radicals by transferring charges between organic molecules and semiconductors.[3] However, it is extremely challenging to achieve the synthesis of a C–C/C–X bond on semiconductor surfaces by precisely controlling selective radical bond formation, because semiconductors interact with photogenerated radicals unselectively and radicals are only present in certain and limited circumstances.[43] Among various regulatory strategies, combining a semiconductor with a matched cocatalyst, such as a metal cluster or single metal atom, to realize a solar-driven radical controllable reaction is a feasible approach. Studies have shown that atomically dispersed cocatalysts have the merits of both homogeneous catalysts and heterogeneous catalysts, including tunable interactions with ligands, well-defined active sites, high stability and excellent recyclability.[44,45] Particularly, these active sites with special electronic structures and unsaturated coordination bonds exert positive effects on the adsorption and activation of reactant molecules.[44,46,47] At the reactive sites, atomically dispersed cocatalysts can manipulate radical transformation for divergent synthesis of target products.[42]

2.3 The impact of surface chemistry in QDs

As shown in Fig. 3a and b, changing the size of QDs can facilely regulate their band gap and the redox potentials of photogenerated electrons and holes,[48,49] which means that the substrate distribution can be adjusted by regulating the organic redox path. Fig. 3c depicts the approximate redox potentials of several typical organic substrates. Theoretically, an organic substrate can be oxidized by semiconductors with the VB maximum higher than its redox potential or be reduced by semiconductors with the CB minimum lower than its own redox potential. Virtually, because of the external environment or unfavorable dynamic, certain organic conversion reactions are still challenging to take place under the bandgap-matching semiconductor catalysis. Modulating the size of semiconductor QDs can effectively change the band gap width and redox potential, thus increasing their thermodynamic feasibility. Cd-rich semiconductor QDs based on III–VI elements are known for their tunable band gap, and have a wider band gap than bulk semiconductors (*i.e.*, about 2.43 eV band gap energy for bulk CdS and 2.65 eV for QDs) due to quantum confinement effects.[51–53] Additionally, the surface properties of QDs can significantly affect their exciton kinetics for the reason that the surface atoms of QDs make up the majority of total atoms.[54,55] In particular, the spatially separated charge carriers can transfer to the semiconductor QD surface independently, and ultimately be captured by molecules adsorbed on their surface or transfer to the reactive sites on the other semiconductors or cocatalysts.[56,57]

In addition to QD size, ligand modification, surface reconstruction, and the active sites also contribute significantly to the promotion of photoredox organic transformation. The interaction between QDs and electron donors/acceptors is enhanced by plentiful surface sites, which encourage the interfacial charge transfer rate of photocatalysis.[58] Generally, QDs provide abundant catalytic active sites and adsorption centers because of their unique surface structural and adjustable atomic proportions. Furthermore, the quantity of acceptor molecules adsorbed on the QD surface is positively correlated with the efficiency of energy transfer. For example, QD gels, once deprived of the surface ligands, exhibit superior photocatalytic activity due to more exposed active sites which improve the probability of reactant adsorption and promote charge transfer.[59] On one hand, constructing a great quantity of surface active sites is of great significance for greatly improving photocatalytic organic conversion, enabling effective reactants and adsorption rapid charge transfer. On the other hand, the application of selective organic conversion can be further expanded by surface structure reconstruction, such as changing the atomic composition and introducing defect vacancies or cocatalysts.

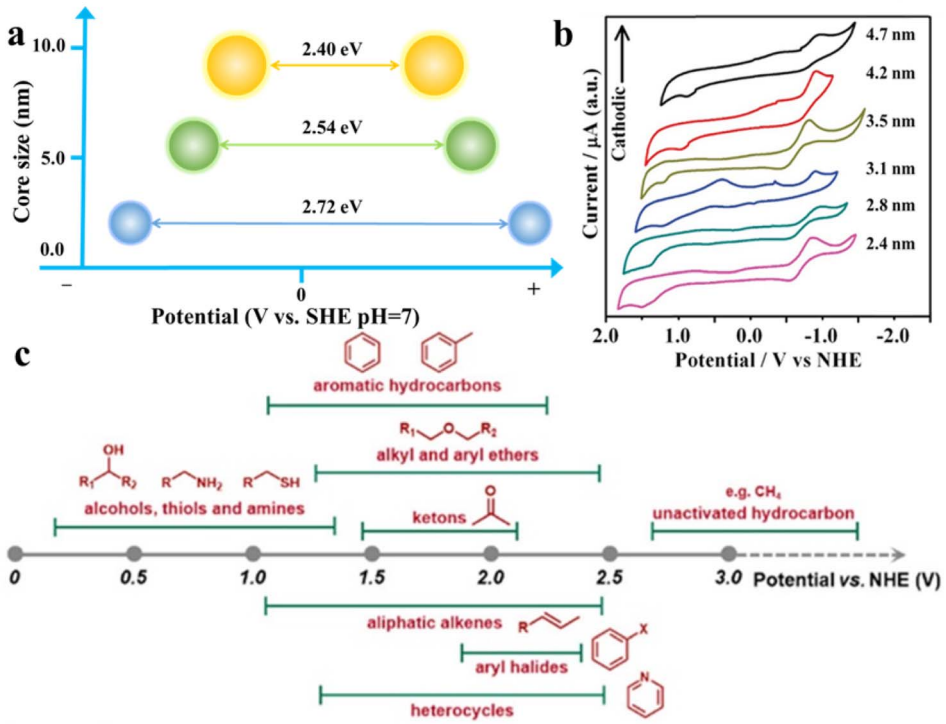

Fig. 3 (a) Illustration of the relationship between the core size and band gap of CdS QDs. (b) Cyclic voltammograms (CVs) on CdTe QDs of different sizes in methylene chloride. Scan rates were 100 mV s^{-1} for all the cases. Reprinted with permission from ref. 50. (c) Approximate redox potential of common chemical molecules. Reprinted with permission from ref. 3.

Additionally, organic/inorganic ligands of QDs have a decisive influence on their surface properties, which can functionalize the QD surface and regulate the charge transfer on semiconductor QDs, thus improving the organic conversion rate in photocatalysis.[32,39,60–63] The primary functions of ligands include: (i) serving as a stabilizer to prevent quantum dots from gathering, (ii) promoting exciton delocalization and interparticle charge transmission,[64,65] (iii) establishing a stable channel for electron transfer between catalysts and metal ions, metal atoms, or other organic molecules,[66,67] and (iv) modulating the properties of catalysts through modification of the surface chemistry.[68–70] Particularly, it has been shown that there is efficient charge transfer between organic molecules and surface ligands of QDs.[71,72] For example, Weiss *et al.* constructed hybrid monolayers of oleate and octyl phosphonate to make the ligand shell of CdS QDs disordering. The unique ligand shell is beneficial to facilitate the hole-transfer step which increases the initial rate and enhances the energy efficiency of the C–C coupled reaction.[61] Studies have shown that the photocatalytic performance of semiconductor QDs can also be greatly influenced by the length, hydrophilicity/hydrophobicity, intrinsic charge properties, and anchoring groups of surface ligands.[30,73,74] For instance, a novel electron tunneling photosystem using surface ligands as the charge transfer medium has been reported. The ligands can not only induce electrostatic self-assembly to construct composite catalysts, but also precisely regulate the directional charge flow of photoredox organic conversion.[75] The surface of transition metal chalcogenide quantum dots (TMC QDs) is negatively charged due to the deprotonation of carboxyl groups of mercaptoacetic acid (MAA) ligands, while the surface of metal nanocrystals (NYs) is positively charged because of partial protonation of the exocyclic nitrogen atoms of 4-dimethylaminopyridine (DMAP) ligands.[76–78] The interfacial insulating electron tunneling layer, which is composed of layered ligands on the surface of TMC QDs (CdSe and CdS) and NYs (Pd and Au), is beneficial to the unidirectional transfer of electrons from QDs to metal nanocrystals, enhancing the carrier lifetime and promoting charge separation.

3. Applications of QDs for photoredox organic transformation

Under mild reaction conditions, using exhaustless solar energy to drive selective photochemical reactions is an environmentally friendly route that can be potentially applied in various industrial organic transformation processes.[79–81] As one of the semiconductor photocatalysts, semiconductor QDs are widely used in photocatalysis such as CO_2 photoreduction, water splitting, degradation of organic pollutants, and organic redox reactions due to their inherent strengths in light absorption, exciton generation, and carrier transfer.[3,9,36,82–84] In this context, the surface modification of QDs with different ligands[30,85] and/or suitable cocatalysts[86,87] can effectively adjust the surface composition and charge distribution of catalysts, thus improving the performance of photocatalysts and improving

the photocatalytic reaction efficiency.[42] In this section, we will focus on the recent advances of QD-based photocatalysts in various photoredox selective organic transformation reactions.

3.1 Reduction of nitroaromatics

As a kind of indispensable organic intermediates, amino aromatic compounds are used to prepare industrial products, such as medicines, dyestuff, pesticides, and pigments,[88–90] and can be synthesized by photocatalytic reduction of different nitroaromatics. Fig. 4 shows that amino aromatic compounds can be synthesized by a direct method through intermediates of *N*-phenylhydroxylamine and nitrosobenzene, or by the condensation method through hydrazobenzene, azobenzene, and azoxybenzene.[91,92] Table 1 summarizes the recent applications for selective photoreduction of nitroaromatics over diverse QD-based photocatalysts. Conventional reduction of nitroaromatics usually involves reducing nitroaromatic compounds to amines by a mild and efficient method with viologens as the electron-transfer catalyst along with the generation of by-products.[93] CdS QDs sealed with mercaptoethylamine hydrochloride (MEA) have been reported to be effective in reducing aromatic nitro compounds to the corresponding aromatic amines without generating the by-products from carbonyl and cyano functional group reduction on the aromatic ring.[94] To further explore the underlying mechanism of aromatic nitro reduction, Weiss's group reported that benzylamine (NB) can be reduced to aniline (NA) over CdS QD photocatalysts through six sequential photoinduced, proton-coupled electron transfers, which can be depicted as a straightforward kinetic model comprising three sequential processes (Fig. 5a).[26] Gas chromatography-mass spectrometry (GC-MS) has detected both four- and six-electron photoproducts of phenylhydroxylamine (PHA) and AN without the two-electron intermediate nitrosobenzene (NSB) (Fig. 5a and b), which is mainly due to the lower reduction potential (+0.29 V) of NSB to PHA, causing the irreversible conversion of the NSB intermediate to the further reduced product PHA. Limited by the production and utilization of a single electron in the QD catalyst under typical photon flux illumination, the photocatalytic reaction mechanism of benzylamine is presented in Fig. 5c.

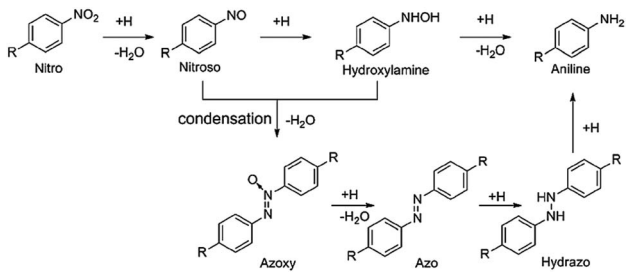

Fig. 4 Mechanism of reduction for catalytic nitroaromatic to aniline. Reprinted with permission from ref. 91.

In one instance, an efficient charge-transfer channel for the reduction of nitroaromatics has been constructed on the (3D) CdSe QD–graphene (GR) nanocomposites by tightly bonding CdSe QDs and GR nanosheets through a universal layer-by-layer self-assembly strategy.[32] The significantly enhanced photoredox performance of this QD-based composite can be attributed to a conjunction of several factors, including the greatly improved separation of photogenerated excitons and the significantly increased specific surface area caused by seamless GR encapsulation,[100–102] thus leading to the superior photocatalytic activity. The obtained results indicated that compared with blank CdSe QDs, the photoactivity of the CdSe QDs-1% GR nanocomposite for selective photoreduction of 4-nitroaniline (4-NA) to 4-phenylenediamine (4-PDA) was markedly enhanced. In addition, it was discovered that the CdSe QDs are universal in nitroaromatic reduction by investigating diverse aromatic nitro compounds possessing various function groups.

Combining QDs with other suitable semiconductor materials (*e.g.*, CdS, ZnSe, and TiO_2) to construct QD-based heterostructures has been regarded as a feasible strategy for prolonging the lifetime of photogenerated excitons and promoting the separation/transfer of charge carriers. For instance, He and co-workers successfully constructed CdSe QD-decorated TiO_2 with exposed facets (CS-T001) for the first time through a facile method, and proved that it was a stable photocatalyst with high activity for nitroaromatic reduction under visible light.[77] Fig. 5d displays the mechanism of photocatalytic

Table 1 Summary of nitroaromatic reduction over QD-based photocatalysts

Entry	Photocatalyst	Atmosphere	Solvent	Scavenger	Light source	Ref.
1	C dots/CdS	N_2	H_2O	$HCOON_4$	3 W LED lamp, $\lambda > 420$ nm	95
2	CdS QDs	Ar	H_2O/CH_3OH	MPA[a]	7 mW 405 nm laser	26
3	CdSe QDs-T001[b]b	N_2	H_2O	Na_2SO_3	500 W Xe-lamp, 420–800 nm	77
4	GQDs/TCN[c]	Vacuum	H_2O	*t*-BuOH, $K_2S_2O_8$, EDTA	300 W Xe-lamp, 320 nm $\leq \lambda \leq$ 780 nm	96
5	N-GQDs[d]	Ar	H_2O	$NaBH_4$	NIR light	97
6	CdSe QDs-GR[e]	N_2	H_2O	Na_2SO_3	300 W Xe-lamp, $\lambda > 420$ nm	32
7	CdTe QDs/GR	N_2	H_2O	Na_2SO_3	300 W Xe-lamp, $\lambda > 420$ nm	27
8	CdS QDs	N_2	D_2O/CD_3OD	Methanol	Blue LED, 450–460 nm	98
9	NYs/TMC QDs[f]	N_2	H_2O	Na_2SO_3	300 W Xe-lamp, $\lambda > 420$ nm	75
10	CdS QDs-In[g]	N_2	H_2O	$HCOON_4$	500 W Xe-lamp, 420–800 nm	99

[a] MPA refers to 3-mercaptopropionic acid. [b] T001 refers to anatase TiO_2 with exposed facets. [c] GQDs/TCN stands for graphene quantum dots/Mn–N–TiO_2/g-C_3N_4. [d] N-GQDs refers to nitrogen-doped graphene quantum dots. [e] GR refers to graphene. [f] NYs refers to metal nanocrystals (Au and Pd) and TMCs refers to transition metal chalcogenides (CdSe and CdS). [g] In metal nanocrystals InOOH.

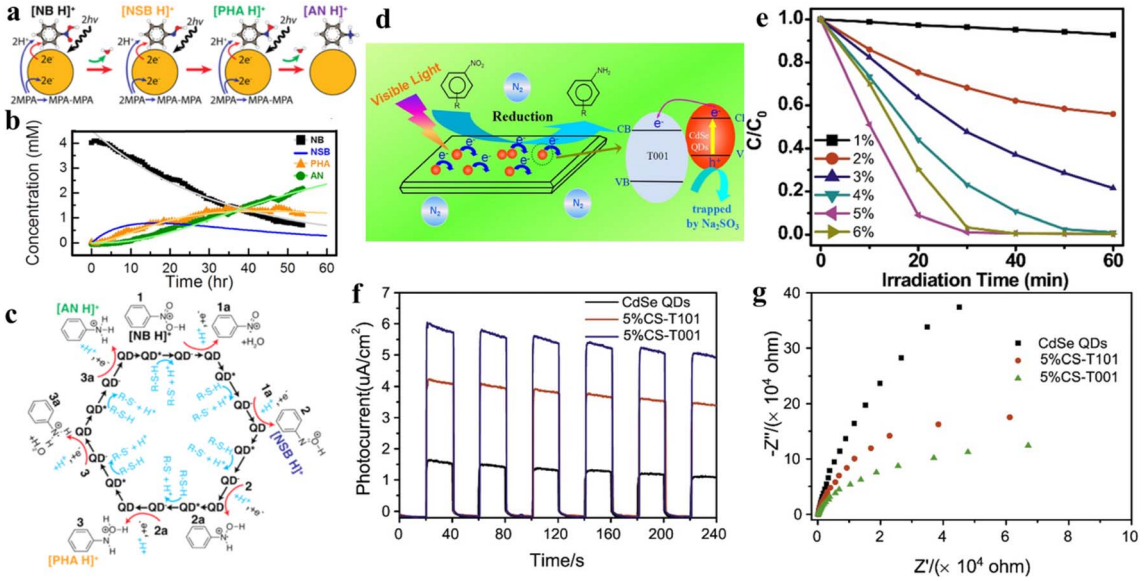

Fig. 5 (a) Catalytic steps of conversion of nitrobenzene to aniline with six-electron, six-proton photoreduction. (b) The relationship between the concentration of NB and reduction products and time. (c) Six sequential proton coupled electron transfer steps of photocatalytic reduction of protonated NB to AN over QDs, with intermediates of NSB and PHA. Reprinted with permission from ref. 26. (d) Illustration for nitroaromatic photoreduction over CS-T001. (e) Photocatalytic performance for reduction of 4-NA over CS-T001 with different contents of CdSe QDs. (f) Transient photocurrent spectra of CS-T001. (g) EIS Nyquist curves. Reprinted with permission from ref. 77.

conversion of nitroaromatics to amino aromatics over CS-T001. The photocatalytic activity of composite catalysts for the reduction of nitroaromatics 4-NA tothe corresponding amino aromatics under ambient conditions has been investigated in the presence of Na_2SO_3 as a cavity scavenger and N_2 purging. Fig. 6e shows that the photocatalytic activity of CS-T001 increases significantly as the content of CdSe QDs increases from 1% to 5%, which indicates that the content of CdSe QDs will affect the composite photocatalytic performance. It is further found that the proper content of CdSe QDs results in uniform particle dispersion on TiO_2 and excellent visible light absorption. Transient photocurrent spectroscopy shows that the photocurrent responses of 5%CS-T001 are significantly enhanced, indicating that the transfer and separation efficiency

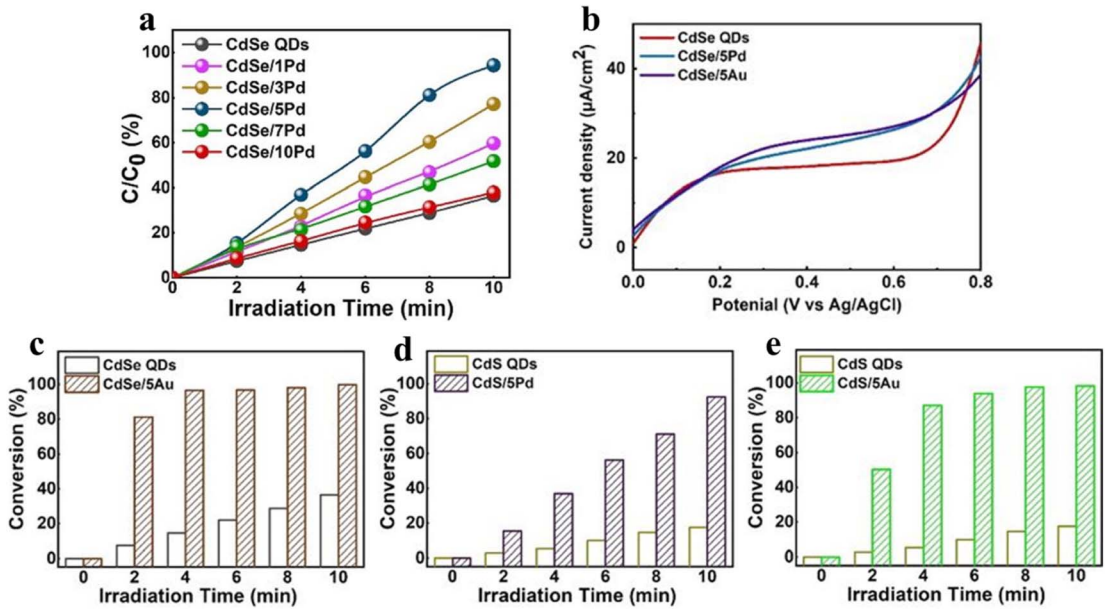

Fig. 6 (a) Photoactivity of selective nitroaromatic reduction over CdSe/Pd nanocomposites with different volume of Pd nanocrystals. (b) LSV plots. Nitroaromatic conversion over (c) CdSe/5Au, (d) CdS/5Pd and (e) CdS/5Au compared to their corresponding single QDs. Reprinted with permission from ref. 75.

of photogenerated charge carriers is higher in 5%CS-T001 compared with CdSe QDs (Fig. 5f). As can be seen from Fig. 5g, the impedance arc radius of 5%CS-T001 is the smallest in all samples, indicating that 5%CS-T001 has a better electrical conductivity, which is conducive to improving transfer of photogenerated charge carriers and thus boosting the photocatalytic efficiency.

Additionally, modifying QDs with other cocatalysts has been regarded as a promising strategy, which promotes the photocatalytic stability and activity by inhibiting the recombination of photogenerated charge carriers. Generally, precious metals (*e.g.*, Pt, Au, and Pd) are the most prevalent cocatalysts, which are deposited on the QD surface to form Schottky junctions at the interface, facilitating the separation of charge carriers and ultimately enhancing the photocatalytic performance. For instance, Xiao and co-workers have designed transition metal chalcogenide QD heterojunction catalysts under ambient conditions *via* a simple ligand-induced electrostatic self-assembly method, exhibiting excellent photocatalytic performance for nitroaromatic reduction due to the improved photogenerated electron transfer and the enhanced response of visible light.[75] As can be seen from Fig. 6a, under visible light irradiation, the blank CdSe QDs exhibit lower photoactivity than Pd-decorated CdSe QDs, which is caused by the fast electron–hole recombination rate. The photocatalytic activities of CdSe/5Au, CdS/5Pd, and CdS/5Au exhibit a similar enhancement trend compared with their corresponding single counterparts under the same conditions (Fig. 6b–e). This result implies the universal roles of the positively charged surface ligand capped metal nanocrystals in facilitating the interfacial charge transport. As seen in Fig. 6b, owing to the higher electron–hole pair recombination rate, the blank CdSe QDs exhibit a weak photocurrent response under visible light irradiation, while the photocurrents of CdSe/5Pd and CdSe/5Au are relatively enhanced because of the enhanced charge separation due to unidirectional electron transport of CdSe induced by electron tunneling.

3.2 Oxidation of alcohol

Selective oxidation of alcohols to aldehydes, ketones, carboxylic acids or C–C coupling products has wide and various industrial applications, such as aldehydes and C–C coupled compounds have a wide utilization in confectionary, beverage, fragrance, and pharmaceutical industries.[103–106] Nevertheless, traditional conversion of alcohols is not only affected by excessive oxidation and toxic oxidants like chromates and manganese oxides, but also requires harsh operating conditions.[107,108] It is expected that QDs with finely tuned redox potentials can be used as photocatalysts to solve the above problems. Table 2 summarizes the recent advances for selective oxidation of alcohols to carbonyl compounds or coupling products over diverse QD-based photocatalysts.

3.2.1. Oxidation of alcohols to aldehydes or ketones. Reactions of alcohols to aldehydes or ketones by selective oxidation is one of the most basic and common functional group conversion processes in fine chemical synthesis.[102,109–111] In most cases, carbonyl compounds are common products of photocatalytic oxidation of alcohols. Taking photocatalytic benzyl alcohol (BA) as an example, Bian *et al.* hprepared an efficient composite photocatalyst consisting of CdS QDs and a TiO_2 mesocrystal with exposed facets (CdS/TiO_2) for the selective oxidation of alcohol.[40] For exploring the active radicals and intermediates in the reaction process, control experiments are performed with various radical reagents. As shown in Fig. 7a, after adding terephthalic acid capable of capturing $^{\bullet}OH$ to the reaction system, no obvious change in the reaction process is observed. However, the conversion rate of BA decreases obviously after the addition either of $AgNO_3$ to capture photoelectrons, or methanol to trap photogenerated holes, or a N_2 flow to remove solubilized O_2, or benzoquinone to trap $^{\bullet}O_2^-$. In addition, the calculation of the BA conversion rate constant k and the electron spin resonance (ESR) spectra of $^{\bullet}O_2^-$ radicals trapped by 5,5-dimethyl-1-pyrroline-*N*-oxide (DMPO) further confirm that $^{\bullet}O_2^-$ radicals are present in the BA

Table 2 Summary of alcohol oxidation over QD-based photocatalysts

Entry	Photocatalyst	Solvent	Substrate	Product	Light source	Ref.
1	MPA[a]-CdSe QD	H_2O	BA[b]	BAD[c]	LED, $\lambda = 410$ nm	29
2	CdTe QDs/5%GR	BTF[d]	Aromatic alcohols	Aryl aldehydes	300 W Xe-lamp, $\lambda > 420$ nm	27
3	CdS/SiO_2	CH_3CN	BA	HB[e]	300 W Xe lamp,	112
4	CdS QDs	D_2O/CD_3OD	BA	BAD/HB	2.6 mW, $\lambda = 405$ nm	113
5	NYs/TMCs QDs[f]	BTF	Aromatic alcohols	Aryl aldehydes	300 W Xe-lamp, $\lambda > 420$ nm	75
6	CdS/TNS[g]	CH_3CN	BA	HB	300 W Xe-lamp, $\lambda > 420$ nm	38
7	CdS-MTA[h]	CH_3CN	Aromatic alcohols	Aryl aldehydes	300 W Xe-lamp, $\lambda > 320$ nm	114
8	CdSe QDs-GR[i]	BTF	Aromatic alcohols	Aryl aldehydes	300 W Xe-lamp, $\lambda > 420$ nm	32
9	CdS-TiO_2	BTF	BA	BAD	300 W Xe-lamp, $\lambda > 420$ nm	40
10	CQD	H_2O	BA	BAD	450 W Xe-lamp, $\lambda < 700$ nm	115
11	CdSe/CdS QDs	DMF	Phenylethanol	Pinacol	Blue LED lamp, 450 nm	116
12	MPA-CdSe QDs	H_2O	Isopropanol	Acetone	3 W LED lamp, $\lambda = 410$ nm	74
13	CdSe QDs-TiO_2-$Ni(OH)_2$	Isopropanol/H_2O	Isopropanol	Acetone	High-pressure mercury lamp, $\lambda > 400$ nm	117
14	CdS QDs@α-ZrP	CH_3CN	BA	BAD	55 W Xe-lamp	118

[a] MPA refers to 3-mercaptopropionic acid. [b] BA refers to benzyl alcohol. [c] BAD stands for benzaldehyde. [d] BTF denotes benzotrifluoride. [e] HB refers to hydrobenzoin. [f] NYs refers to metal nanocrystals (Au and Pd) and TMCs refers to transition metal chalcogenides (CdSe and CdS). [g] TNS refers to titanium dioxide nanosheets. [h] CdS-MTA refers to mesoporous CdS-sensitized TiO_2 nanoparticle assemblies. [i] GR refers to graphene.

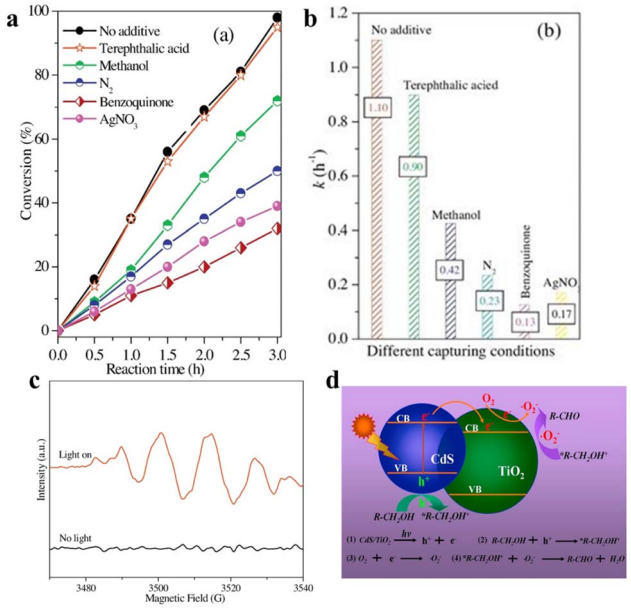

Fig. 7 (a) The conversion of BA photooxidation CdS/TiO_2 in diverse capturers. (b) Photocatalytic rate constant k of BA oxidation under different capturing conditions. (c) ESR spectra. (d) Schematic for photocatalytic selective oxidation of alcohol to aldehyde. Reprinted with permission from ref. 40.

oxidation reaction system, whereas $^{\cdot}OH$ radicals are absent in this system (Fig. 7b and c). The photooxidation mechanism of BA over CdS–TiO_2 based on the above results is shown in Fig. 7d. Upon excitation by visible light, CdS QDs are activated to produce electrons and holes. The photoelectrons are then transferred to TiO_2 *via* the CdS–TiO_2 heterojunctions to activate the solubilized O_2 for $^{\cdot}O_2^-$ radicals, and the holes will activate the adsorbed BA to obtain benzyl alcohol cation radicals which will finally be oxidized by $^{\cdot}O_2^-$ radicals to benzaldehyde.

In addition to the photocatalytic dehydrogenation mechanism of BA above, Wu *et al.* proposed 3-mercaptopropionic acid-capped CdSe QDs that oxidize alcohols to carbonyl compounds. Electron transfer that facilitates the formation of an active thiyl radical is the most critical initial step. The thiyl radical in turn induces the activation of reactant molecules to generate radical intermediates, which then produce the corresponding carbonyl compounds *via* a radical relay process. They have also investigated a variety of aromatic alcohols to explore the universality of alcohol oxidation over CdSe QDs under the same reaction conditions.[29] The results indicate that the photocatalytic conversion of aromatic alcohols on CdSe QDs is independent of the volume of the *ortho*-substituted group of the aryl ring, and the benzyl alcohols substituted by electron-withdrawing groups at the *para*-position has a slightly slower reaction rate than that substituted by electron-donating groups.

3.2.2. Oxidation of alcohols to C–C coupling products. Dehydrogenation coupling of alcohol substrates is very important in current organic chemical synthesis, and has become an ideal strategy for the production of dihydric alcohols or other multi-carbon compounds. In the case of benzyl alcohol (BA), the photocatalytic oxidation of BA to carbonyl compounds or C–C

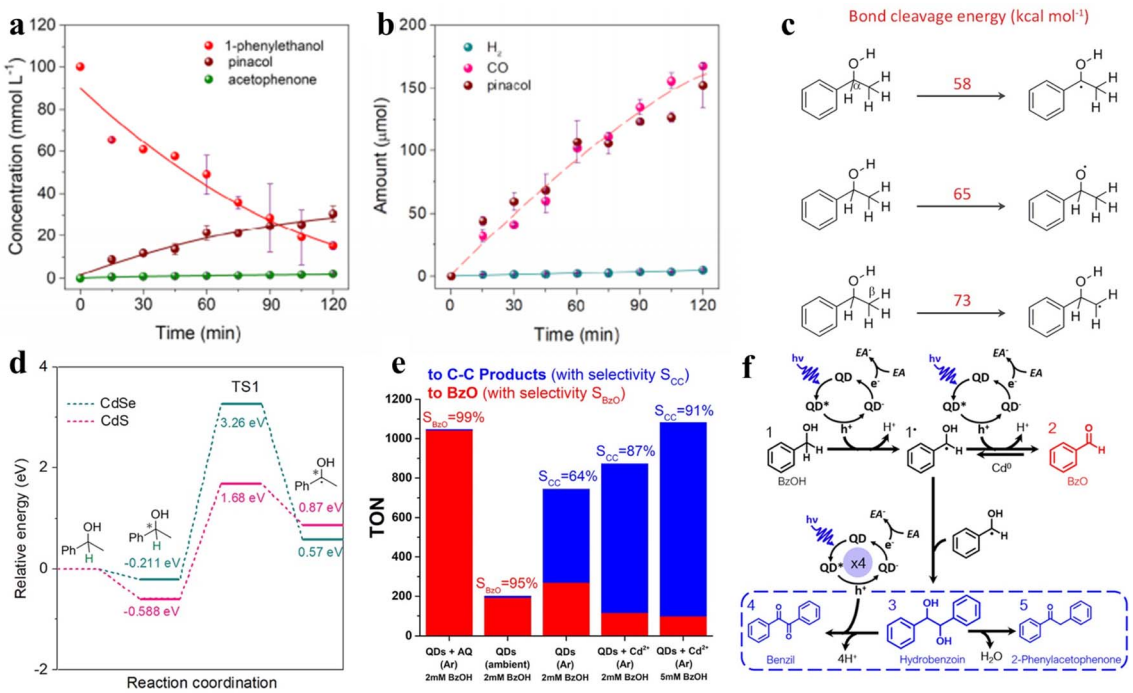

Fig. 8 (a) Concentration changes of 1-phenylethanol, pinacol, and acetophenone during the reaction. (b) The generation of gas products and pinacol with increasing irradiation time. (c) Bond cleavage energy. (d) Full potential energy for 1-phenylethanol deprotonation on CdSe/CdS QDs. Reprinted with permission from ref. 116. (e) Production and selectivity of the photocatalyst. "AQ" refers to sodium anthraquinone-2-sulfonate; "BzOH" refers to benzyl alcohol. "BzO" refers to benzaldehyde. (f) The pathway of photocatalytic BzOH oxidation. "EA" refers to an electron acceptor. Reprinted with permission from ref. 113.

coupling products generally involves the activation of the C–O and O–H bonds of BA, while the cleavage of unreactive C–H bonds and the consequent C–C bond construction are exciting but challenging reactions in the production of value-added chemicals. In 2019, Wu *et al.* reported the photocatalytic oxidation of alcohols for C–C coupling for the synthesis of pinacol and CO_2 photoreduction over CdSe/CdS QDs.[116] According to Fig. 8a and b, the product of pinacol increases significantly as 1-phenylethanol is gradually consumed during the reaction, whereas acetophenone is maintained at an exceedingly low concentration throughout the illumination. Meanwhile, the amount of oxidized product (pinacol) is approximately similar to that of CO, which proves that acetophenone is not an intermediate but a by-product in this system. Moreover, density functional theory (DFT) calculations are performed to investigate the energies of O–H, C_α–H, and C_β–H bonds cleaving into reactive radicals (Fig. 8c). The C_α–H bond shows the lowest bond cleavage energy compared with C_β–H and O–H bonds, suggesting that the C_α–H bond breaks more easily under the same conditions. By further analysis of DFT, the1-phenylethanol is also found to directly bind to the anion vacancies of QDs *via* the substituent, resulting in stronger adsorption (Fig. 8d). Based on the above results, mechanistic studies reveal that the Se and S vacancies on the CdSe/CdS QD surface serve as reactive sites to promote the production of the corresponding pinacols. This surface reaction mechanism presented here is distinguished from the previously reported mechanism of alcohol oxidation *via* a radical relay process.[29]

In another example, Weiss and co-workers achieved photocatalytic oxidation of BA to BAD or C–C coupling products with the selectivity near 100% by adjusting the quantity of Cd on QD surfaces by *in situ* deposition (Fig. 8e).[113] Fig. 8f shows that the photoexcitation of CdS QDs without deposited Cd induces the radical intermediates (1˙) to form BzO (2), while the produced hydrobenzoin (3) sometimes undergoes a four-electron oxidation to benzil (4) over QDs in the presence of metallic cadmium.

Furthermore, our group has constructed a SiO_2-surpported CdS QD (CdS/SiO_2) material for visible-light-driven dehydrogenative C–C coupling reaction of BA under ambient conditions.[112] Fig. 9a shows that hydrogen (H_2) and hydrobenzoin (HB) production rates are evaluated to be *ca.* 1.0, indicating a stoichiometric dehydrogenation reaction. Furthermore, the CdS/SiO_2 photocatalysts exhibit excellent photoactivity with a yield of 84.6% and an outstanding selectivity of near 100%. Meanwhile, high performance liquid chromatography (HPLC) is used to identify the liquid products produced in the photocatalytic system to explore the evolution kinetics of BA, benzaldehyde (BAD) and HB over the CdS/SiO_2 composites. Fig. 9b shows that the BA decreases continuously with the increase in HB and BAD as the reaction proceeds. The mechanism of dehydrocoupling of BA into H_2 and HB is proposed in Fig. 9c. Owing to the intrinsic band-gap optical absorption property of semiconductors, CdS QDs can not only absorb direct incident light but also recycle the scattered light in the near field of SiO_2. Recently, we designed a bifunctional 0D CdS QDs-2D TiO_2 (CdS/TNS) heterostructure for visible-light-driven C–C coupling of BA

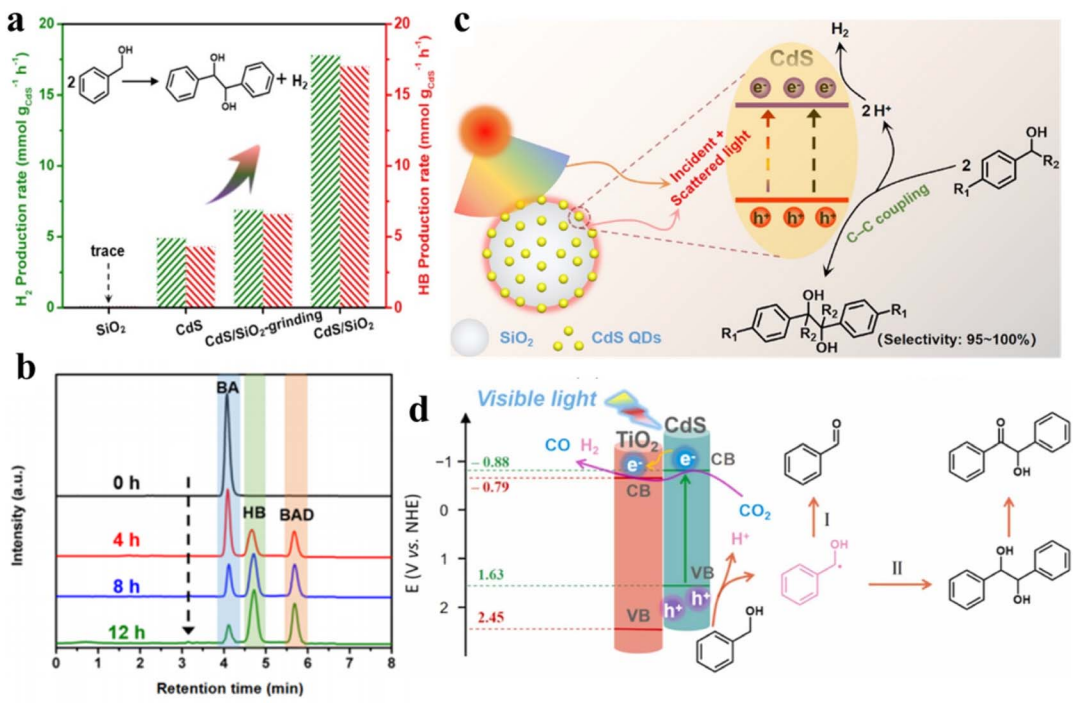

Fig. 9 (a) Production of H_2 and HB over different samples. (b) HPLC spectra of the liquid products during photocatalytic reaction on CdS/SiO_2 composites during photocatalytic reaction. (c) Schematic illustration of CdS QDs/SiO_2 for photocatalytic HB synthesis and H_2 production. Reprinted with permission from ref. 112. (d) Diagram of the photocatalytic reaction mechanism for CO_2 reduction and C–C coupling synthesis over CdS/TNS composites. Reprinted with permission from ref. 38.

along with the photoreduction of CO_2 to CO.[38] The introduction of TNS as the carrier may greatly affect the abstraction of α–H at the interface between QDs and the carrier, thus regulating the selectivity of BA oxidation from BAD to the C–C coupling products. Upon visible-light irradiation, TiO_2 cannot be activated, while CdS QDs are excited to produce high-energy electrons and holes. This type-II heterojunction induces the electrons located in the CB of CdS to be transferred to the CB of TNS, thereby driving the dual-function photocatalytic redox processes (Fig. 9d). Photogenerated holes in the VB of CdS can activate the C–H bonds of BA to produce protons and ˙CH(OH)Ph. This produced ˙CH(OH)Ph radicals will then be oxidized by holes for producing BAD or C–C coupling products. At the same time, the CO_2 molecules and remaining protons are reduced to CO and H_2 by photoexcited electrons.

3.3 C–H functionalization

Recent decades have seen a considerable increase interest in functionalizing C–H bonds in the chemistry of organic synthesis. Particularly, using the activation of C–H to synthesize complex organic structures is a highly efficient reaction strategy.[119,120] However, oxidative C–H bond cleavage sometimes involves the use of toxic and expensive metal oxidants like $Ir(ppy)_2(dtbbpy)X$ and $Ru(bpy)_3X_2$, endangering the sustainable study of C–H activation. In this context, single-sized QDs could replace some traditional catalysts and induce C–H bond activation to promote different photoredox reactions (*e.g.*, β-alkylation, β-aminoalkylation, and amine arylation).[61,121] Moreover, solar-driven C–H functionalization by using CdSe QDs or CdS QDs as catalysts is currently of increasing interest. Here, we will focus on the photocatalytic C–H bond activation to form C–C and C–S bonds from abundant and easily accessible compounds containing X–H bonds.

3.3.1 Alkylation and arylation of an allyl C–H bond. The functionalization of allylic $C(sp^3)$–H enables the functional groups to bind directly to the sp^3 carbon center near the alkene moiety rather than to the more active alkene, offering a common pathway for further processing unactivated $C(sp^3)$–H bonds.[124] The improved redox activity of the QD photocatalysts in electron excited states can efficiently promote the allylic $C(sp^3)$–H functionalization reactions without introducing external reductants and oxidants.

Recently, using QDs as the photocatalyst, Wu's group reported a direct cross-coupling of allylic $C(sp^3)$–H bonds with α-amino C–H bonds or heteroarenes, respectively (Fig. 10a).[122] The formation of an allylic radical can be confirmed by radical-trapping experiments, deuterium experiments, product distribution detection, and electron paramagnetic resonance (EPR) spectroscopy in this catalytic cycle. Under illumination, the allylic $C(sp^3)$–H bonds and α-amino C–H bonds are synchronously activated by photogenerated holes in CdSe QDs to form transient allylic radicals and α-amino alkyl radicals. Later, the intermolecular radical–radical cross coupling promotes the formation of new C–C bonds. Simultaneously, protons generated by C–H bond scission will form H˙ in the CB of CdSe QDs, and the H˙ stably adsorbed on the QD surface will combine to release H_2. Additionally, the allylic radicals can also produce arylation products by reacting with heteroarenes through a Minisci-type mechanism[125] over CdSe QDs(Fig. 10a).[126]

3.3.2 Thiolation of an allyl C–H bond and vinyl C–H bond. Strategies for constructing C–S bonds are mainly to utilize aryl

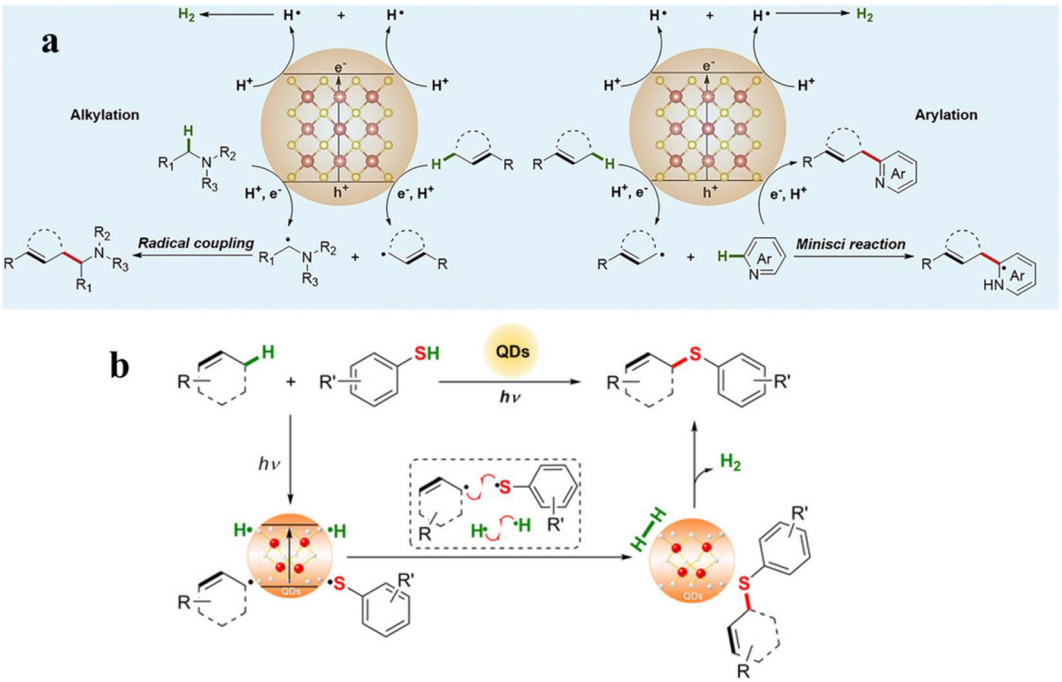

Fig. 10 (a) Alkylation and arylation of an allylic $C(sp^3)$–H bond. Reprinted with permission from ref. 122. (b) Direct activation of an allylic C–H bond to form a C–S bond. Reprinted with permission from ref. 123.

halides and thiols as coupling partners with the help of transition metal catalysts. In addition, C–S bond formation catalyzed by a transition metal successfully overcomes the shortages of conventional synthesis of organosulfur compounds, such as the rapid consumption of a metal catalyst, catalyst deactivation, and harsh reaction conditions.[127,128] Nevertheless, strong interactions between organosulfur compounds and catalysts result in deactivation of catalysts or oxidation of sulfur atoms under oxidizing conditions. In recent years, Wu's group reported visible light driven cobalt-catalyzed and aerobic metal-free catalyzed C–H bond thiolation.[129,130] In 2021, they first reported direct allylic C(sp^3)–H thiolation through cross-coupling of an allylic radical and thiyl radical over CdSe QDs under visible light illumination(Fig. 10b).[123] According to previous reports,[131] allylic C(sp^3)–H was activated under air conditions by an ionic coupling process with the help of disulfide as a hydrogen atom transfer reagent for the generation of a C(sp^3)–S bond. The photochemical reaction strategy proposed by Wu's group has realized the generation of allylic radicals and thiyl radicals through direct activation of allylic C–H and S–H bonds, leaving no need for extraneous oxidants or radical initiators. When introducing vinylic C(sp^2)–H for substitution of allylic C(sp^3)–H to carry out the thiolation, a vinylic C(sp^2)–S bond could also be constructed by direct cross-coupling of C–H and S–H bonds, which is different from the cross-coupling reactions of vinyl halides with thiols and the addition reaction of thiols with alkynes.[132–134]

3.4 Oxidation of sulfides

Oxidation products of sulfides, such as sulfoxide, sulfone, and disulfide, play an important role in chemistry and biology. However, conventional strategies for sulfide oxidation using toxic oxidants or costly reagents with the need for high temperature and unstable reactive intermediates result in reduced selectivity or excessive oxidation of the products. Accordingly, developing a green route for the oxidation of sulfide compounds is necessary.[135–138] Noteworthily, photocatalytic sulfide oxidation over QD-based materials under mild conditions is a promising alternative. For instance, Ford *et al.* found that the CdSe QDs photocatalyzed the oxidative cleavage of 1,1-dithiooxalate (DTO) to produce carbon disulfide.[139] The transfer of photoexcited holes from QDs to surface DTOs triggers this oxidative cleavage reaction.

Recently, CdSe QDs have been reported to induce oxidative coupling of various thiols to produce disulfides and H_2 in the absence of sacrificial reagents or external oxidants under visible light.[142] The photocatalytic conversion of thiols to disulfides and H_2 over CdSe QDs is significantly improved after the addition of nickel(II) salt as a cocatalyst. Even under aerobic conditions, the yield of disulfide and H_2 could reach 92% and 95%, respectively. To demonstrate the photocatalysis of CdSe QDs, the steady-state emission and typical emission decay profiles of CdSe QDs have been used to study the interaction between organic substrates and catalysts. 3-Mercaptopropionic acid (MPA) significantly reduces the band-edge emission of the QDs and accelerates the rate of emission decay (Fig. 11a and b). Furthermore, EPR

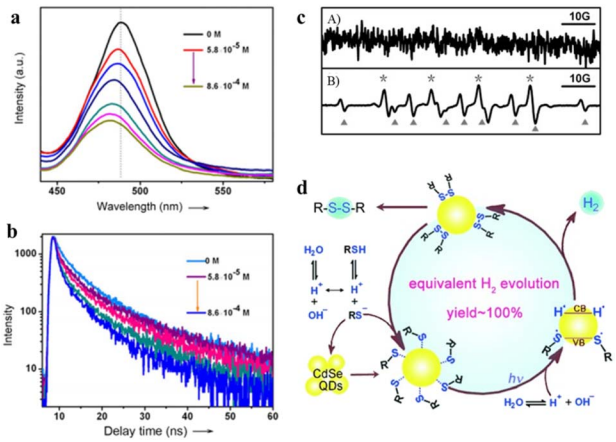

Fig. 11 (a) Steady-state emission spectra of CdSe QDs at different MPA concentrations. (b) The emission decay profiles of CdSe QDs. (c) EPR signals before (A) and after (B) irradiation. (d) Mechanism of photocatalytic oxidation of thiols to disulfides and H_2. Reprinted with permission from ref. 142.

spectroscopy confirms the formation of sulfenyl radicals under illumination. According to the control experiment, no spectral signal can be observed before irradiation, and after 10 s of this irradiation ($\lambda > 400$ nm), the spectral signals (labeled with *) of a typical sulfenyl radical ($RS^{\bullet}$) can be detected (Fig. 11c). Besides, the results of the GC-mass spectrum reveal that the photogenerated sulfenyl radicals are coupled on the CdSe QD surface to generate disulfide products, which then diffuse into the solution. On the basis of the above experimental results, the oxidative coupling mechanism of thiols is proposed in Fig. 11d. Upon illumination, the deprotonated thiols are bound to the surface of CdSe QDs to generate QD/thiolate conjugates containing Cd–S. CdSe QDs are excited by visible light to generate electron–hole pairs and then the adsorbed thiolates reductively quench the excited states of the QDs to produce sulfur-centered radicals ($RS^{\bullet}$), which are coupled on the QD surface to form the corresponding disulfides. Meanwhile, the H^+ is reduced to $H^{\bullet}$ which is stabilized on the QD surfaces to form H_2.

3.5 Oxidation of amines

Amines are oxidized to synthesize various value-added products including nitriles, oximes, amides, and imines, which constitute the key N-containing building blocks in the contemporary chemical industry. In particular, imines, as important organic synthesis intermediates, play a vital role in the industrial production of fine chemicals like dyestuff and pharmaceuticals. The preparation of imines can be achieved by photocatalytic conversion of amine compounds under aerobic conditions.[143,144] For example, Kim and co-workers developed an efficient and facile synthesis strategy to regulate the photocatalytic performance of heteroatom-doped graphene quantum dots (GQDs) by controlling the dopant.[140] As shown in Fig. 12a, compared with nitrogen- and oxygen-doped GQDs, nitrogen/sulfur codoped GQDs exhibit much higher activity of photocatalysis for the aerobic oxidative coupling reaction of

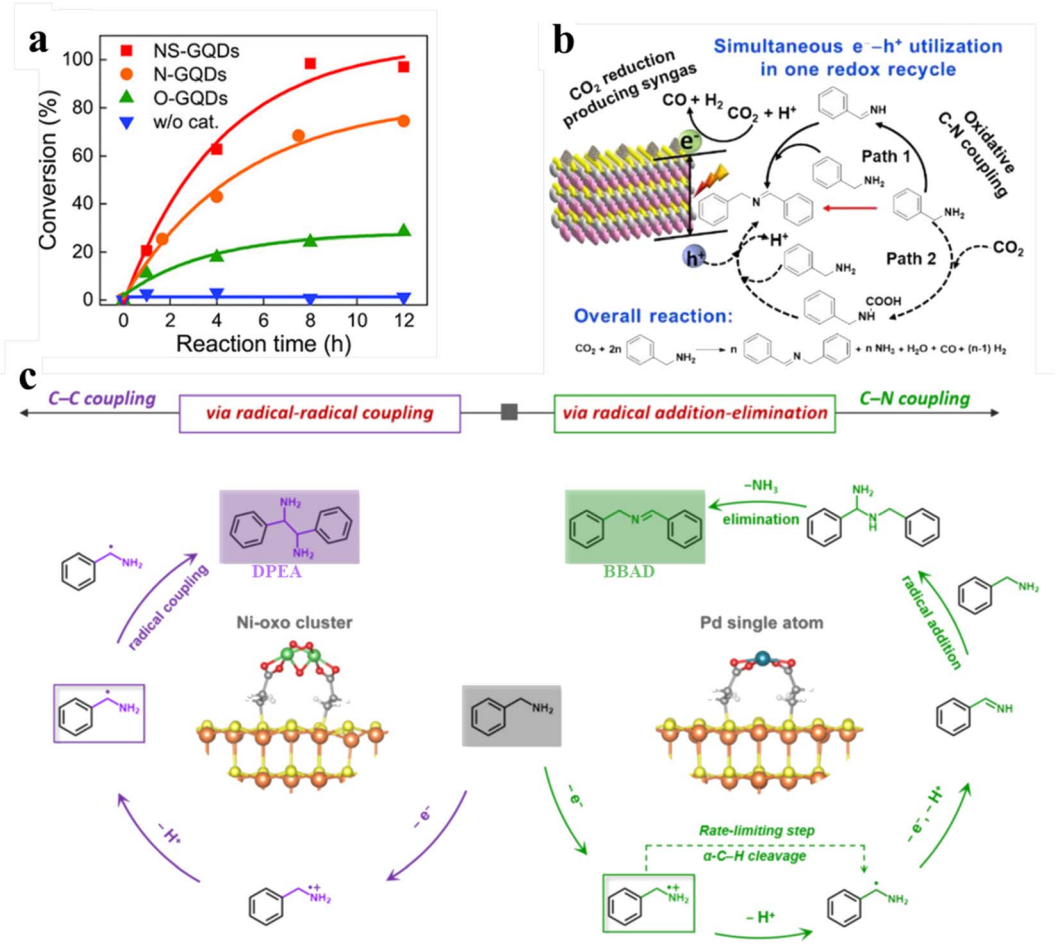

Fig. 12 (a) Conversion of benzylamine over NS-GQDs, N-GQDs, and O-GQDs. Reprinted with permission from ref. 140. (b) Illustration of photocatalytic selective benzylamine oxidation integrated with CO_2 reduction over (BP/ZIS) heterostructures. Reprinted with permission from ref. 141. (c) Mechanism diagram of photocatalytic selective oxidative coupling of benzylamine over different samples. Reprinted with permission from ref. 42.

benzylamine. Besides, Zhu *et al.* studied in detail the catalytic activity of oxygen-rich carbon quantum dots for aerobic oxidation of amines.[146] Li *et al.*, recently, have designed multifunctional graphene QDs decorated with a tertiary amine functional group. Under visible light illumination GQD-DMA exhibits excellent activity and higher photocatalytic efficiency for amine oxidative coupling.[147]

Furthermore, our group has reported using a simple electrostatic interaction assembly method to immobilize black phosphorus quantum dots (BP QDs) on the surface of $ZnIn_2S_4$ nanosheets (ZIS NSs) to construct BP QDs-$ZnIn_2S_4$ (BP/ZIS) heterostructures for oxidative C–N coupling integrated with CO_2 reduction (Fig. 12b).[141] The experimental results demonstrate that the effective charge transformation in this heterostructure promotes the separation of charge carriers, thereby enhancing the photoactivity of the composite photocatalyst. Very recently, we prepared an atomically dispersed Ni or Pd-decorated CdS/SiO_2 composite through *in situ* photodeposition on the CdS QD surface for the selective photochemical coupling of amines (Fig. 12c).[42] Atomically dispersed metal atoms act as reactive sites to manipulate the unselective photogenerated radical conversion to precisely control the dehydrocoupling reaction of benzylamine to C–C or C–N coupling products with excellent activity and selectivity. Specifically, Ph($^{\bullet}$CH)NH_2 can produce vicinal diamines through direct C–C coupling over Ni-oxo cluster decorated catalysts, while the Ph(CH)NH produced by the dehydrogenation of Ph($^{\bullet}$CH)NH_2 can produce imines by C–N coupling over single Pd atom decorated catalysts. SiO_2-supported CdS QDs can catalyze the dehydrocoupling of benzylamine to 1,2-diphenylethylenediamine (DPEA) paired with H_2 production under Xe-lamp irradiation. When decorating with Ni, the rate of both H_2 evolution and DPEA formation of the Ni-CdS/SiO_2 composites improve. Particularly, Ni–CdS/SiO_2 can achieve a yield of 90% with the selectivity near 100% after 7 h irradiation. Upon decorating with Pd, Pd–CdS/SiO_2 promotes the evolution of H_2 and also modulates the selectivity of benzylamine oxidation from DPEA to *N*-benzylbenzaldimine (BBAD). Their selectivity approaches 100% when it reaches a BBAD production rate of 22.1 mmol g_{CdS}^{-1} h^{-1}. Moreover, the yield of BBAD on Pd–CdS/SiO_2 can reach 99% after 6 h of irradiation.

3.6 Biomass valorization

3.6.1 Reforming of lignocellulosic biomass. As the most abundant and accessible biological resource, lignocellulosic biomass, consisting of lignin, cellulose, and hemicellulose (Fig. 13a), possesses enormous potential towards sustainable production of chemical feedstocks and fuels.[3,148–150] However, several catalytic systems for the conversion of lignocellulosic biomass (*e.g.*, gasification, hydrolysis, liquefaction, pyrolysis and deoxygenation/hydrogenation) commonly result in very complex products. Thus, it is necessary to develop a reaction system with simple operation, concentrated product distribution and excellent catalytic activity to overcome the current problems.[149,151]

Metal sulfide QDs, which can effectively catalyze the breaking of C–C or C–O bonds in lignocellulosic biomass, have made some progress in photocatalytic conversion of natural lignin.[145,152] For instance, Reisner *et al.* proposed the application of semiconductor CdS QDs for light-driven transformation of hemicellulose, lignin, and cellulose to H_2 in alkaline aqueous solution.[148] Recently, Wang *et al.* developed a method of solubilizing a catalyst to convert natural lignin in birch wood meal with the help of the colloidal nature of CdS QDs.[150] Under mild reaction conditions, the selective cleavage of the β-O-4 bond can be induced by CdS QDs with the generation of a C_α radical intermediate *via* the electron–hole coupled (EHCO) mechanism (Fig. 13b),[145,150] which consuming both photogenerated electrons and holes. The main products found in the liquid phase after reaction are functionalized aromatic monomers such as syringyl-derived ketones (S-ketones) and guaiacyl-derived ketones (G-ketones). Subsequently, Wang and co-workers also explored with different surface ligands the effect of different surface ligands for photocatalytic conversion of native lignin over QDs.[30] Specifically, the hydrophilic organic ligands make the CdS QDs to be pseudo homogeneous in polar CH_3OH/H_2O solution, which allows the intimate contact of QDs with the reactant, thus increasing the conversion efficiency of native birch lignin. Instead, the hydrophobic ligands cause CdS QDs to readily aggregate in solvents so that the native lignin conversion rate is not satisfactory (Fig. 13c). In addition, with the decrease in the length of mercaptoalkanoic acid ligands on CdS QDs, the production of aromatic monomers increases (Fig. 13d). The kinetic curves of electron decay indicate that the length of mercaptoalkanoic acid ligands is firmly relevant to the photocatalytic performance of CdS QDs (Fig. 13e). Further kinetic studies reveal that the charge carriers of CdS QDs can be transferred to the β-O-4 bond of native lignin *via* organic ligands.[30]

3.6.2 Conversion of lignin models. Owing to the structural complexity of natural lignin polymers, most research efforts have chosen simple and readily available model compounds with typical lignin characteristic chemical bonds to test novel catalysts and explore the reaction mechanism.[145] A number of semiconductor photocatalysts used for lignin model compound

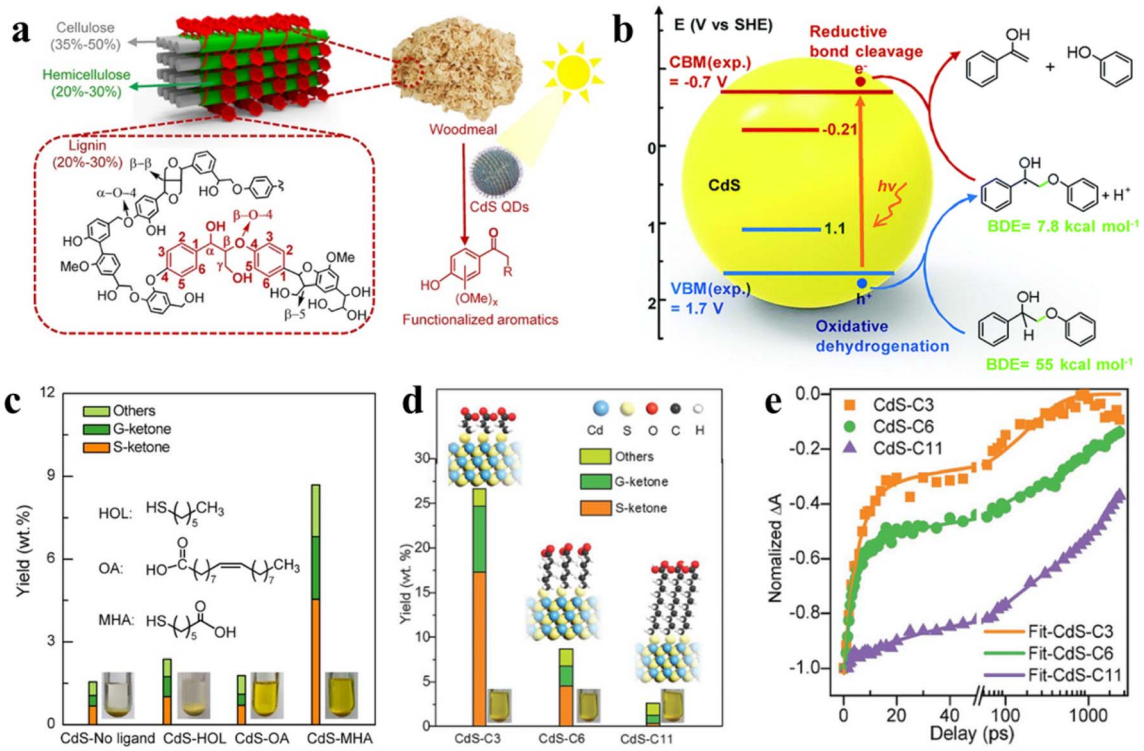

Fig. 13 (a) Diagram of the lignocellulose structure. Reprinted with permission from ref. 30. (b) EHCO mechanism for photocatalytic conversion of a dimeric β-O-4 model over CdS QDs. Reprinted with permission from ref. 145. (c) Effect of different surface ligands on photocatalytic valorization of birch woodmeal over CdS QDs. (d) Effect of the length of surface ligands on photocatalytic valorization of birch woodmeal over CdS QDs. (e) Transient absorption spectroscopy. Reprinted with permission from ref. 30.

conversion have been investigated so far.[153–156] Semiconductor QDs, in particular, have been getting widespread attention over recent years. One of the most commonly used lignin model compounds is 2-phenoxy-1-phenylethanol (PP-ol), which is structurally simple and readily analyzed.[145,155,157] For example, compared with TiO_2, Cu_2O, $BiVO_4$, ZnS, CuS, and graphitic C_3N_4, Wang *et al.* reported that CdS nanoparticles (NPs) exhibit unique photoactivity in the cleavage of the β-O-4 bond of PP-ol.[150] However, the results of activity experiments indicate that the photoactivity of CdS QDs for PP-ol conversion is apparently higher compared to that of CdS NPs. Moreover, various lignin model compounds can be selectivity catalyzed over CdS QDs for the cleavage of the β-O-4 bond, while the other oxygenic functional groups (*e.g.*, methoxy, phenol, and ketone groups) remain largely unchanged.

In another example, Cossairt *et al.* demonstrated that the QDs are versatile for C_α–O bond cleavage of lignin model substrates.[73] The lignin model substrates are oxidized or photochemically reduced from benzylic alcohol to 4′-methoxyacetophenone or guaiacol by phenyl ketone intermediates. Moreover, with the help of QD photocatalysts, the lignin model substrates can be successfully converted to obtain the cleavage products without unnecessary purification steps.

3.6.3 Conversion of biomass-derived furans. A series of downstream products derived from lignocellulose (*e.g.*, furfural (FF), furfuryl alcohol (FA), 2,5-dimethylfuran (2,5-DMF), 2-methylfuran (2-MF), 5-hydroxymethylfurfural (HMF), *etc.*) can be yielded after the initial treatment of biomass feedstocks. These products can act as source materials to produce high value added products through solar powered catalytic reprocessing.[3,158] For, instance, Wang *et al.* used Ru-doped $ZnIn_2S_4$ as a catalyst for acceptorless dehydrogenative C–C coupling of lignocellulose-derived methylfurans to coproduce H_2 and diesel fuel precursors under visible light.[159] Our group has prepared $Ti_3C_2T_x$/CdS composite catalysts for photocatalytic furfural alcohol conversion in the water phase to produce H_2 and value-added furfural.[160] In recent years, Wu and Xiong *et al.* made some progress in converting biomass derivatives over semiconductor QD catalysts with concomitant evolution of H_2 or CO_2 under mild reaction conditions.[41,161,162]

Recently, Wu's group demonstrated that semiconductor QDs can interact with tetrahydrofuran (THF) to form CdSe QDs/THF conjugates for photocatalytic selective direct α-C–H bond activation of THF under mild conditions.[161] Control experiments and spectroscopic studies prove that the QDs/THF conjugates are formed by combining the oxygen atom of THF with the "vacant sites" of the QD surface. The mechanism for

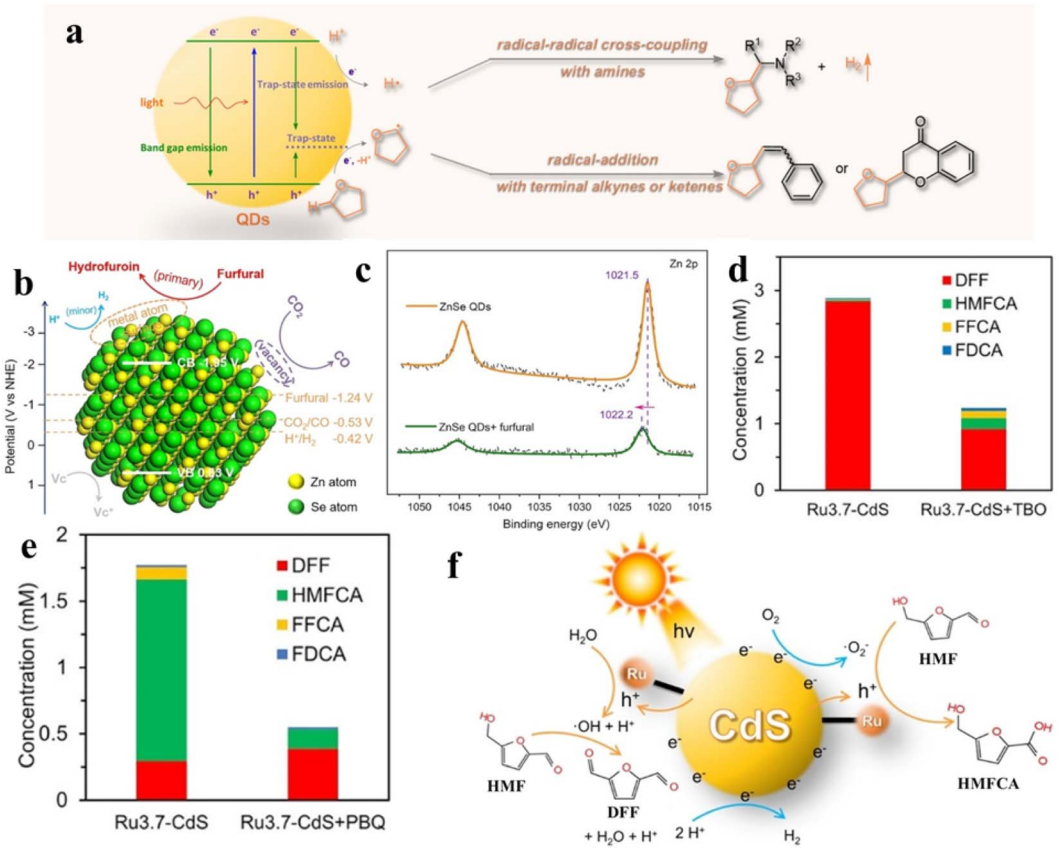

Fig. 14 (a) Schematic diagram of the activation of THF on QD surfaces. Reprinted with permission from ref. 161. (b) Mechanism of furfural inhibiting H_2 production over ZnSe QDs. (c) X-ray photoelectron spectroscopy (XPS) spectra. Reprinted with permission from ref. 162. Concentration of the products from photocatalytic HMF oxidation over Ru-CdS catalysts (d) under an Ar atmosphere and (e) under an air atmosphere. (f) The mechanism of photocatalytic oxidation of HMF over Ru-CdS. Reprinted with permission from ref. 41.

photocatalytic conversion of THF over QDs/THF conjugates is depicted in Fig. 14a. The adsorbed THF molecules are oxidized by photogenerated holes into alkoxyalkyl radicals, while the protons produced by oxidative cleavage of the α-C–H bonds of THF are reduced by photogenerated electrons into H atoms. Then, the produced alkoxyalkyl radical directly undergoes radical cross-coupling with an α-amino radical from the amino C(sp^3)–H bond or radical addition with alkene or phenylacetylene (Fig. 14a). Besides the coupling and addition reactions of THF, Wu *et al.* also presented the ZnSe QDs in the C–C coupling of furfural and revealed that furfural at exposed QD metal sites blocks the competitive reaction (H_2 evolution) in photocatalytic CO_2 reduction (Fig. 14b).[162] According to the mechanistic analysis, the furfural coupling occurs at the exposed surface Zn-sites of QDs, consuming the electrons and protons initially devoted to produce H_2. Fig. 14c shows a positive shift in the Zn 2p XPS binding energy after adding furfural into the solution of ZnSe QDs, indicating that the charge density decreases. That is attributed to the migration of electrons from surface Zn to furfural, that is, furfural competes with protons for photogenerated electrons simultaneously. According to the above results, furfural can effectively inhibit the production of H_2 over ZnSe QDs.

In addition, Xiong and co-workers designed a novel photocatalyst by anchoring a Ru complex on CdS QDs for selective oxidation of HMF with excellent photocatalytic activity and selectivity.[41] The Ru complex can effectively extract photogenerated holes of CdS QDs, thus remarkably improving the photostability of CdS and providing moderate oxidation capacity. By adding different radical scavengers in different atmospheres, it is further proved that the product selectivity of HMF oxidation is intimately connected to $^{\bullet}OH$ and $^{\bullet}O_2^-$ radicals. As displayed in Fig. 14d, under an Ar atmosphere, when *tert*-butanol (TBO) consuming $^{\bullet}OH$ is added to the reaction solution, the conversion of HMF to DFF is significantly suppressed. The results suggest that DFF is produced by $^{\bullet}OH$. Similarly, *p*-benzoquinone (PBQ) is added to consume $^{\bullet}O_2^-$ under an air atmosphere. It can be found that $^{\bullet}O_2^-$ has an impact on the generation of HMFCA and FFCA (Fig. 14e). Through further experimental studies, the catalytic mechanism schematic as shown in Fig. 14f is proposed. The photogenerated holes on CdS QDs are transferred to the Ru complex for the oxidation of water to generate $^{\bullet}OH$ under an Ar atmosphere. Instead, $^{\bullet}O_2^-$ is produced by combining photogenerated electrons with O_2 on catalysts under an air atmosphere.

4. Conclusions and perspectives

In this review, we discuss the current status of photocatalysis in selective organic synthesis over semiconductor QD-based materials. After briefly introducing the fundamental principles of photoredox organic transformation of QD-based catalysts and the effects of surface chemistry on photocatalytic performance of QDs, we focus on the recent advances in various QD-mediated photoredox organic conversion reactions including nitroaromatic reduction, selective alcohols oxidation, C–H functionalization, sulfide oxidation, amine oxidation, and biomass valorization. Photocatalytic organic conversion based on QDs has made plenty of achievements and has a broad prospect of research. However, research in this area is still in its infancy with both opportunities and several long-standing challenges needing continuous efforts to promote future innovation in organic synthesis on semiconductor QDs.

First, the performance of QD catalysts currently used in photoredox catalysis is unsatisfactory. By integrating QDs with cocatalysts, semiconductors, and/or carbon materials, decorating with organic/inorganic ligands, or constructing core/shell hybrid composites, it is promising to develop methods of QD functionalization for more efficient photocatalysts with structural modifiability, exciton controllability, and surface tunability. Generally, improving the activity and selectivity of organic conversion over QD-based photocatalysts can be roughly started from the following aspects: (i) enhancing light absorption and improving light utilization efficiency, (ii) boosting carrier separation/transfer and facilitating surface reaction kinetics, and (iii) manipulating radicals and/or intermediates to form target products. For example, QDs can recycle the scattered light in the near-field of SiO_2 through interface interaction to enhance light-harvesting[112] or can realize effective charge immigration by engineering intimate interfacial contact *via* constructing a type II heterostructure or forming a QD conjugate, thus further promoting the photocatalytic performance over QD-based catalysts.

Second, the construction of a cooperative photoredox reaction system for combining oxidative organic synthesis with H_2 evolution or CO_2 reduction deserves more attention due to the limited activity and selectivity of traditional single-functional photocatalytic reactions. On one hand, in order to select suitable catalysts and construct an efficient catalytic system, the band structure suitable for both oxidation and reduction reactions, the active sites for this dual-functional photoredox reactions, and the efficiency of electron and hole separation and transfer need to be considered. On the other hand, it is necessary to screen the organic substrates matching the energy band of catalysts and take the interaction among organic substrates, radical intermediates, and the photocatalyst surface into consideration to allow the photoexcited holes and electrons on the QD-based catalysts to be consumed simultaneously to produce value-added chemicals and solar fuels such as CO and H_2.

Third, continues efforts are needed to enhance the selectivity of target products in the dual-functional photocatalytic system. The selectivity of an organic synthesis reaction can be modulated by optimizing the external reaction conditions including temperature, solvent, light source, reaction time and so on. For example, the $^{\bullet}O_2^-$ derived from O_2 in air can manipulate the organic intermediates to produce specific products, which cannot occur in an inert atmosphere. The catalyst modification strategy is also an effective approach to improve the selectivity of organic synthesis. Since the interaction between semiconductor QDs and photogenerated radicals is unselective, the radical conversion can be manipulated by rational design of QD-based catalysts to accurately control the selectivity of organic synthesis reactions, such as cationic/anionic ratio

variation, ligand exchange, doping with heteroatoms, and hybridization with cocatalysts or other matchable semiconductors to construct stable heterostructures. The photoredox reaction kinetics can be promoted by regulating the band structure, adjusting the molecular adsorption sites and improving the surface chemical structure.

Last but not least, QDs-based catalysts are multicomponent materials in that a layer of organic ligands inevitably exists on the surface of inorganic core, thus making the system much more complex. To this end, the potential mechanism of various photocatalytic organic transformations over QDs remains to be explored. *In situ* comprehensive studies can monitor the changes of the structure and surface valence states of the photocatalyst, explore the intermediates formed during the photocatalytic organic conversion reaction, and identify the rate-limiting step, which assist the exploration of the reaction mechanism of diverse redox organic transformations over QD-based photocatalysts. Further study of the organic synthesis mechanism is practically necessary to reveal the influence of material morphology, structure, composition, reaction conditions and other related factors on the efficiency and selectivity of organic conversion of QD-based catalysts, and offers a new sparkling idea for the more rational design and development of QD-based artificial photocatalysts.

Conflicts of interest

There are no conflicts to declare.

Acknowledgements

The support from the National Natural Science Foundation of China (NSFC) (22172030, 22072023, 21872029, U1463204, and 21173045), the Program for National Science and Technology Innovation Leading Talents (00387072), the Program for Leading Talents of Fujian Universities, the first Program of Fujian Province for Top Creative Young Talents, and the Natural Science Foundation of Fujian Province (2017J07002 and 2019J01631) is acknowledged.

References

1 P. Riente and T. Noël, *Catal. Sci. Technol.*, 2019, **9**, 5186–5232.
2 J.-Y. Li, Y.-H. Li, M.-Y. Qi, Q. Lin, Z.-R. Tang and Y.-J. Xu, *ACS Catal.*, 2020, **10**, 6262–6280.
3 M.-Y. Qi, M. Conte, M. Anpo, Z.-R. Tang and Y.-J. Xu, *Chem. Rev.*, 2021, **121**, 13051–13085.
4 R. Akiyama and S. Kobayashi, *Chem. Rev.*, 2009, **109**, 594–642.
5 D. M. Schultz and T. P. Yoon, *Science*, 2014, **343**, 1239176.
6 T. P. Yoon, M. A. Ischay and J. Du, *Nat. Chem.*, 2010, **2**, 527–532.
7 H. Kisch, *Angew. Chem., Int. Ed.*, 2013, **52**, 812–847.
8 M. Cherevatskaya, M. Neumann, S. Füldner, C. Harlander, S. Kümmel, S. Dankesreiter, A. Pfitzner, K. Zeitler and B. König, *Angew. Chem., Int. Ed.*, 2012, **51**, 4062–4066.
9 X.-B. Li, C.-H. Tung and L.-Z. Wu, *Nat. Rev. Chem.*, 2018, **2**, 160–173.
10 Y. Yuan, N. Jin, P. Saghy, L. Dube, H. Zhu and O. Chen, *J. Phys. Chem. Lett.*, 2021, **12**, 7180–7193.
11 H. H. Wei, C. M. Evans, B. D. Swartz, A. J. Neukirch, J. Young, O. V. Prezhdo and T. D. Krauss, *Nano Lett.*, 2012, **12**, 4465–4471.
12 R. D. Harris, S. Bettis Homan, M. Kodaimati, C. He, A. B. Nepomnyashchii, N. K. Swenson, S. Lian, R. Calzada and E. A. Weiss, *Chem. Rev.*, 2016, **116**, 12865–12919.
13 J. Luo, S. Zhang, M. Sun, L. Yang, S. Luo and J. C. Crittenden, *ACS Nano*, 2019, **13**, 9811–9840.
14 M. S. Kodaimati, K. P. McClelland, C. He, S. Lian, Y. Jiang, Z. Zhang and E. A. Weiss, *Inorg. Chem.*, 2018, **57**, 3659–3670.
15 K. V. Vokhmintcev, P. S. Samokhvalov and I. Nabiev, *Nano Today*, 2016, **11**, 189–211.
16 H. Lu, Z. Huang, M. S. Martinez, J. C. Johnson, J. M. Luther and M. C. Beard, *Energy Environ. Sci.*, 2020, **13**, 1347–1376.
17 Q. Shen, K. Katayama and T. Toyoda, *J. Energy Chem.*, 2015, **24**, 712–716.
18 Y. Barak, I. Meir, A. Shapiro, Y. Jang and E. Lifshitz, *Adv. Mater.*, 2018, **30**, 1801442.
19 W. M. Witzel, A. Shabaev, C. S. Hellberg, V. L. Jacobs and A. L. Efros, *Phys. Rev. Lett.*, 2010, **105**, 137401.
20 R. J. Ellingson, M. C. Beard, J. C. Johnson, P. Yu, O. I. Micic, A. J. Nozik, A. Shabaev and A. L. Efros, *Nano Lett.*, 2005, **5**, 865–871.
21 C. R. Kagan, L. C. Bassett, C. B. Murray and S. M. Thompson, *Chem. Rev.*, 2021, **121**, 3186–3233.
22 H. Zhu, Y. Yang and T. Lian, *Acc. Chem. Res.*, 2013, **46**, 1270–1279.
23 A. J. Nozik, M. C. Beard, J. M. Luther, M. Law, R. J. Ellingson and J. C. Johnson, *Chem. Rev.*, 2010, **110**, 6873–6890.
24 Y. Yang, W. Rodríguez-Córdoba and T. Lian, *Nano Lett.*, 2012, **12**, 4235–4241.
25 S. J. O. Hardman, D. M. Graham, S. K. Stubbs, B. F. Spencer, E. A. Seddon, H.-T. Fung, S. Gardonio, F. Sirotti, M. G. Silly, J. Akhtar, P. O'Brien, D. J. Binks and W. R. Flavell, *Phys. Chem. Chem. Phys.*, 2011, **13**, 20275–20283.
26 S. C. Jensen, S. Bettis Homan and E. A. Weiss, *J. Am. Chem. Soc.*, 2016, **138**, 1591–1600.
27 S. Hou, M.-H. Huang, Y.-B. Li, S. Xu, X. Lin, X.-Y. Fu and F.-X. Xiao, *Inorg. Chem.*, 2020, **59**, 16654–16664.
28 Y. Li, T.-T. Zhuang, F. Fan, O. Voznyy, M. Askerka, H. Zhu, L. Wu, G.-Q. Liu, Y.-X. Pan, E. H. Sargent and S.-H. Yu, *Nat. Commun.*, 2018, **9**, 4947.
29 L.-M. Zhao, Q.-Y. Meng, X.-B. Fan, C. Ye, X.-B. Li, B. Chen, V. Ramamurthy, C.-H. Tung and L.-Z. Wu, *Angew. Chem., Int. Ed.*, 2017, **56**, 3020–3024.
30 X. Wu, S. Xie, C. Liu, C. Zhou, J. Lin, J. Kang, Q. Zhang, Z. Wang and Y. Wang, *ACS Catal.*, 2019, **9**, 8443–8451.
31 A. Pal, I. Ghosh, S. Sapra and B. König, *Chem. Mater.*, 2017, **29**, 5225–5231.
32 M.-H. Huang, X.-C. Dai, T. Li, Y.-B. Li, Y. He, G. Xiao and F.-X. Xiao, *J. Phys. Chem. C*, 2019, **123**, 9721–9734.
33 F.-X. Xiao, J. Miao, H.-Y. Wang and B. Liu, *J. Mater. Chem. A*, 2013, **1**, 12229–12238.

34 Y. Jiang, C. Wang, C. R. Rogers, M. S. Kodaimati and E. A. Weiss, *Nat. Chem.*, 2019, **11**, 1034–1040.
35 J. Hu, T.-J. Pu, Z.-W. Xu, W.-Y. Xu and Y.-S. Feng, *Adv. Synth. Catal.*, 2019, **361**, 708–713.
36 C. Huang, X.-B. Li, C.-H. Tung and L.-Z. Wu, *Chem.–Eur. J.*, 2018, **24**, 11530–11534.
37 Y. Yuan, H. Zhu, K. Hills-Kimball, T. Cai, W. Shi, Z. Wei, H. Yang, Y. Candler, P. Wang, J. He and O. Chen, *Angew. Chem., Int. Ed.*, 2020, **59**, 22563–22569.
38 M.-Y. Qi, Q. Lin, Z.-R. Tang and Y.-J. Xu, *Appl. Catal., B*, 2022, **307**, 121158.
39 Z.-W. Xi, L. Yang, D.-Y. Wang, C.-D. Pu, Y.-M. Shen, C.-D. Wu and X.-G. Peng, *J. Org. Chem.*, 2018, **83**, 11886–11895.
40 X. Li, J. Wang, Y. Men and Z. Bian, *Appl. Catal., B*, 2016, **187**, 115–121.
41 T. Xia, W. Gong, Y. Chen, M. Duan, J. Ma, X. Cui, Y. Dai, C. Gao and Y. Xiong, *Angew. Chem., Int. Ed.*, 2022, **61**, e202204225.
42 M.-Y. Qi, M. Conte, Z.-R. Tang and Y.-J. Xu, *ACS Nano*, 2022, **16**, 17444–17453.
43 S. Wang, S. Tang and A. Lei, *Sci. Bull.*, 2018, **63**, 1006–1009.
44 C. Gao, J. Low, R. Long, T. Kong, J. Zhu and Y. Xiong, *Chem. Rev.*, 2020, **120**, 12175–12216.
45 S. Ji, Y. Chen, S. Zhao, W. Chen, L. Shi, Y. Wang, J. Dong, Z. Li, F. Li, C. Chen, Q. Peng, J. Li, D. Wang and Y. Li, *Angew. Chem., Int. Ed.*, 2019, **58**, 4271–4275.
46 L. Wang, W. Zhang, S. Wang, Z. Gao, Z. Luo, X. Wang, R. Zeng, A. Li, H. Li, M. Wang, X. Zheng, J. Zhu, W. Zhang, C. Ma, R. Si and J. Zeng, *Nat. Commun.*, 2016, **7**, 14036.
47 Z. Liu, F. Huang, M. Peng, Y. Chen, X. Cai, L. Wang, Z. Hu, X. Wen, N. Wang, D. Xiao, H. Jiang, H. Sun, H. Liu and D. Ma, *Nat. Commun.*, 2021, **12**, 6194.
48 A. M. Smith and S. Nie, *Acc. Chem. Res.*, 2010, **43**, 190–200.
49 D. A. Wheeler and J. Z. Zhang, *Adv. Mater.*, 2013, **25**, 2878–2896.
50 S. K. Haram, A. Kshirsagar, Y. D. Gujarathi, P. P. Ingole, O. A. Nene, G. B. Markad and S. P. Nanavati, *J. Phys. Chem. C*, 2011, **115**, 6243–6249.
51 F.-K. Shang, M.-Y. Qi, C.-L. Tan, Z.-R. Tang and Y.-J. Xu, *ACS Phys. Chem. Au*, 2022, **2**, 216–224.
52 X. Lin, S.-H. Li, K.-Q. Lu, Z.-R. Tang and Y.-J. Xu, *New J. Chem.*, 2018, **42**, 14096–14103.
53 M.-H. Sun, M.-Y. Qi, Z.-R. Tang and Y.-J. Xu, *Appl. Catal., B*, 2023, **321**, 122019.
54 S. V. Kilina, P. K. Tamukong and D. S. Kilin, *Acc. Chem. Res.*, 2016, **49**, 2127–2135.
55 J. Jasieniak and P. Mulvaney, *J. Am. Chem. Soc.*, 2007, **129**, 2841–2848.
56 S. Chen, Y. Qi, C. Li, K. Domen and F. Zhang, *Joule*, 2018, **2**, 2260–2288.
57 E. Hofman, R. J. Robinson, Z.-J. Li, B. Dzikovski and W. Zheng, *J. Am. Chem. Soc.*, 2017, **139**, 8878–8885.
58 S. V. Kershaw, L. Jing, X. Huang, M. Gao and A. L. Rogach, *Mater. Horiz.*, 2017, **4**, 155–205.
59 D. Liu, J. Nyakuchena, R. Maity, X. Geng, J. P. Mahajan, C. C. Hewa-Rahinduwage, Y. Peng, J. Huang and L. Luo, *Chem. Commun.*, 2022, **58**, 11260–11263.
60 E. A. Weiss, *ACS Energy Lett.*, 2017, **2**, 1005–1013.
61 Z. Zhang, K. Edme, S. Lian and E. A. Weiss, *J. Am. Chem. Soc.*, 2017, **139**, 4246–4249.
62 Y. Zhu, T. Jin, T. Lian and E. Egap, *J. Chem. Phys.*, 2021, **154**, 204903.
63 K. A. Perez, C. R. Rogers and E. A. Weiss, *Angew. Chem., Int. Ed.*, 2020, **59**, 14091–14095.
64 A. Nag, D. S. Chung, D. S. Dolzhnikov, N. M. Dimitrijevic, S. Chattopadhyay, T. Shibata and D. V. Talapin, *J. Am. Chem. Soc.*, 2012, **134**, 13604–13615.
65 X.-B. Li, B. Liu, M. Wen, Y.-J. Gao, H.-L. Wu, M.-Y. Huang, Z.-J. Li, B. Chen, C.-H. Tung and L.-Z. Wu, *Adv. Sci.*, 2016, **3**, 1500282.
66 Y. Bao, J. Wang, Q. Wang, X. Cui, R. Long and Z. Li, *Nanoscale*, 2020, **12**, 2507–2514.
67 B. M. Graff, B. P. Bloom, E. Wierzbinski and D. H. Waldeck, *J. Am. Chem. Soc.*, 2016, **138**, 13260–13270.
68 P. R. Brown, D. Kim, R. R. Lunt, N. Zhao, M. G. Bawendi, J. C. Grossman and V. Bulović, *ACS Nano*, 2014, **8**, 5863–5872.
69 L. K. Putri, B.-J. Ng, W.-J. Ong, H. W. Lee, W. S. Chang, A. R. Mohamed and S.-P. Chai, *Appl. Catal., B*, 2020, **265**, 118592.
70 M. A. Boles, D. Ling, T. Hyeon and D. V. Talapin, *Nat. Mater.*, 2016, **15**, 141–153.
71 T. X. Ding, J. H. Olshansky, S. R. Leone and A. P. Alivisatos, *J. Am. Chem. Soc.*, 2015, **137**, 2021–2029.
72 J. H. Olshansky, T. X. Ding, Y. V. Lee, S. R. Leone and A. P. Alivisatos, *J. Am. Chem. Soc.*, 2015, **137**, 15567–15575.
73 M. J. Enright, K. Gilbert-Bass, H. Sarsito and B. M. Cossairt, *Chem. Mater.*, 2019, **31**, 2677–2682.
74 X.-B. Fan, S. Yu, X. Wang, Z.-J. Li, F. Zhan, J.-X. Li, Y.-j. Gao, A.-D. Xia, Y. Tao, X.-B. Li, L.-P. Zhang, C.-H. Tung and L.-Z. Wu, *Adv. Mater.*, 2019, **31**, 1804872.
75 X. Lin, Z.-Q. Wei, Q.-L. Mo, S. Hou, S. Xu, X.-Y. Fu and F.-X. Xiao, *J. Catal.*, 2021, **400**, 28–39.
76 P. Wang, D. Li, J. Chen, X. Zhang, J. Xian, X. Yang, X. Zheng, X. Li and Y. Shao, *Appl. Catal., B*, 2014, **160–161**, 217–226.
77 P. Wang, X. Li, J. Fang, D. Li, J. Chen, X. Zhang, Y. Shao and Y. He, *Appl. Catal., B*, 2016, **181**, 838–847.
78 D. I. Gittins and F. Caruso, *Angew. Chem., Int. Ed.*, 2001, **40**, 3001–3004.
79 M.-Q. Yang, N. Zhang, M. Pagliaro and Y.-J. Xu, *Chem. Soc. Rev.*, 2014, **43**, 8240–8254.
80 F.-K. Shang, Y.-H. Li, M.-Y. Qi, Z.-R. Tang and Y.-J. Xu, *Catal. Today*, 2023, **410**, 85–101.
81 A. Li, W. Zhu, C. Li, T. Wang and J. Gong, *Chem. Soc. Rev.*, 2019, **48**, 1874–1907.
82 H.-L. Wu, X.-B. Li, C.-H. Tung and L.-Z. Wu, *Adv. Mater.*, 2019, **31**, 1900709.
83 G. Gao, Q. Xi, H. Zhou, Y. Zhao, C. Wu, L. Wang, P. Guo and J. Xu, *Nanoscale*, 2017, **9**, 12032–12038.
84 R. S. Selinsky, Q. Ding, M. S. Faber, J. C. Wright and S. Jin, *Chem. Soc. Rev.*, 2013, **42**, 2963–2985.

85 X. Zhu, Y. Lin, J. San Martin, Y. Sun, D. Zhu and Y. Yan, *Nat. Commun.*, 2019, **10**, 2843.
86 B. Pal, T. Torimoto, K.-i. Okazaki and B. Ohtani, *Chem. Commun.*, 2007, **5**, 483–485.
87 X.-B. Li, C.-H. Tung and L.-Z. Wu, *Angew. Chem., Int. Ed.*, 2019, **58**, 10804–10811.
88 C. Chu, S. Rao, Z. Ma and H. Han, *Appl. Catal., B*, 2019, **256**, 117792.
89 C. Zhang, T. Li, J. Zhang, S. Yan and C. Qin, *Appl. Catal., B*, 2019, **259**, 118030.
90 C. M. Malengreaux, S. L. Pirard, J. R. Bartlett and B. Heinrichs, *Chem. Eng. J.*, 2014, **245**, 180–190.
91 W.-Z. Gao, Y. Xu, Y. Chen and W.-F. Fu, *Chem. Commun.*, 2015, **51**, 13217–13220.
92 H.-U. Blaser, *Science*, 2006, **313**, 312–313.
93 C. Yu, B. Liu and L. Hu, *J. Org. Chem.*, 2001, **66**, 919–924.
94 P. Eskandari, F. Kazemi and Z. Zand, *J. Photochem. Photobiol., A*, 2014, **274**, 7–12.
95 N.-N. Chai, H.-X. Wang, C.-X. Hu, Q. Wang and H.-L. Zhang, *J. Mater. Chem. A*, 2015, **3**, 16613–16620.
96 Y.-C. Nie, F. Yu, L.-C. Wang, Q.-J. Xing, X. Liu, Y. Pei, J.-P. Zou, W.-L. Dai, Y. Li and S. L. Suib, *Appl. Catal., B*, 2018, **227**, 312–321.
97 H. Liu, H. Wang, Y. Qian, J. Zhuang, L. Hu, Q. Chen and S. Zhou, *ACS Appl. Nano Mater.*, 2019, **2**, 7043–7050.
98 A. W. Mureithi, Y. Sun, T. Mani, A. R. Howell and J. Zhao, *Cell Rep. Phys. Sci.*, 2022, **3**, 100889.
99 P. Wang, X. Zhou, Y. Shao, D. Li, Z. Zuo and X. Liu, *J. Colloid Interface Sci.*, 2021, **601**, 186–195.
100 C. Han, Z. Chen, N. Zhang, J. C. Colmenares and Y.-J. Xu, *Adv. Funct. Mater.*, 2015, **25**, 221–229.
101 A. K. Geim, *Science*, 2009, **324**, 1530–1534.
102 Y. Zhang, Z.-R. Tang, X. Fu and Y.-J. Xu, *ACS Nano*, 2011, **5**, 7426–7435.
103 G. Palmisano, E. García-López, G. Marcì, V. Loddo, S. Yurdakal, V. Augugliaro and L. Palmisano, *Chem. Commun.*, 2010, **46**, 7074–7089.
104 M. Addamo, V. Augugliaro, M. Bellardita, A. Di Paola, V. Loddo, G. Palmisano, L. Palmisano and S. Yurdakal, *Catal. Lett.*, 2008, **126**, 58–62.
105 S. Caron, R. W. Dugger, S. G. Ruggeri, J. A. Ragan and D. H. B. Ripin, *Chem. Rev.*, 2006, **106**, 2943–2989.
106 T. Mallat and A. Baiker, *Chem. Rev.*, 2004, **104**, 3037–3058.
107 G. Palmisano, V. Augugliaro, M. Pagliaro and L. Palmisano, *Chem. Commun.*, 2007, 3425–3437.
108 M. Zhang, Q. Wang, C. Chen, L. Zang, W. Ma and J. Zhao, *Angew. Chem., Int. Ed.*, 2009, **48**, 6081–6084.
109 Q. Wang, M. Zhang, C. Chen, W. Ma and J. Zhao, *Angew. Chem., Int. Ed.*, 2010, **49**, 7976–7979.
110 C. Aellig, C. Girard and I. Hermans, *Angew. Chem., Int. Ed.*, 2011, **50**, 12355–12360.
111 Y. Zhang, N. Zhang, Z.-R. Tang and Y.-J. Xu, *Chem. Sci.*, 2012, **3**, 2812–2822.
112 M.-Y. Qi, Y.-H. Li, M. Anpo, Z.-R. Tang and Y.-J. Xu, *ACS Catal.*, 2020, **10**, 14327–14335.
113 K. P. McClelland and E. A. Weiss, *ACS Appl. Energy Mater.*, 2019, **2**, 92–96.
114 I. Tamiolakis, I. N. Lykakis and G. S. Armatas, *Catal. Today*, 2015, **250**, 180–186.
115 H. Li, R. Liu, S. Lian, Y. Liu, H. Huang and Z. Kang, *Nanoscale*, 2013, **5**, 3289–3297.
116 Q. Guo, F. Liang, X.-B. Li, Y.-J. Gao, M.-Y. Huang, Y. Wang, S.-G. Xia, X.-Y. Gao, Q.-C. Gan, Z.-S. Lin, C.-H. Tung and L.-Z. Wu, *Chem*, 2019, **5**, 2605–2616.
117 S. Yu, Z.-J. Li, X.-B. Fan, J.-X. Li, F. Zhan, X.-B. Li, Y. Tao, C.-H. Tung and L.-Z. Wu, *ChemSusChem*, 2015, **8**, 642–649.
118 G. Borah, A. Borborah and N. Gogoi, *Bull. Mater. Sci.*, 2022, **45**, 136.
119 T. G. Frihed, M. Bols and C. M. Pedersen, *Eur. J. Org. Chem.*, 2016, **2016**, 2740–2756.
120 N. Sauermann, T. H. Meyer, Y. Qiu and L. Ackermann, *ACS Catal.*, 2018, **8**, 7086–7103.
121 J. A. Caputo, L. C. Frenette, N. Zhao, K. L. Sowers, T. D. Krauss and D. J. Weix, *J. Am. Chem. Soc.*, 2017, **139**, 4250–4253.
122 C. Huang, J. Qiao, R.-N. Ci, X.-Z. Wang, Y. Wang, J.-H. Wang, B. Chen, C.-H. Tung and L.-Z. Wu, *Chem*, 2021, **7**, 1244–1257.
123 C. Huang, R.-N. Ci, J. Qiao, X.-Z. Wang, K. Feng, B. Chen, C.-H. Tung and L.-Z. Wu, *Angew. Chem., Int. Ed.*, 2021, **60**, 11779–11783.
124 Q. Cheng, H.-F. Tu, C. Zheng, J.-P. Qu, G. Helmchen and S.-L. You, *Chem. Rev.*, 2019, **119**, 1855–1969.
125 R. S. J. Proctor and R. J. Phipps, *Angew. Chem., Int. Ed.*, 2019, **58**, 13666–13699.
126 Q.-J. Yao and B.-F. Shi, *Chem*, 2021, **7**, 1405–1406.
127 N. Sundaravelu, S. Sangeetha and G. Sekar, *Org. Biomol. Chem.*, 2021, **19**, 1459–1482.
128 C.-F. Lee, R. S. Basha and S. S. Badsara, *Top. Curr. Chem.*, 2018, **376**, 25.
129 G. Liang, J.-H. Wang, T. Lei, Y.-Y. Cheng, C. Zhou, Y.-J. Chen, C. Ye, B. Chen, C.-H. Tung and L.-Z. Wu, *Org. Lett.*, 2021, **23**, 8082–8087.
130 G. Zhang, C. Liu, H. Yi, Q. Meng, C. Bian, H. Chen, J.-X. Jian, L.-Z. Wu and A. Lei, *J. Am. Chem. Soc.*, 2015, **137**, 9273–9280.
131 J. Kim, B. Kang and S. H. Hong, *ACS Catal.*, 2020, **10**, 6013–6022.
132 T. Kondo and T.-a. Mitsudo, *Chem. Rev.*, 2000, **100**, 3205–3220.
133 J. V. Burykina, N. S. Shlapakov, E. G. Gordeev, B. König and V. P. Ananikov, *Chem. Sci.*, 2020, **11**, 10061–10070.
134 N. Velasco, C. Virumbrales, R. Sanz, S. Suárez-Pantiga and M. A. Fernández-Rodríguez, *Org. Lett.*, 2018, **20**, 2848–2852.
135 R. B. Wagh, S. H. Gund and J. M. Nagarkar, *J. Chem. Sci.*, 2016, **128**, 1321–1325.
136 H. Shinkai, K. Maeda, T. Yamasaki, H. Okamoto and I. Uchida, *J. Med. Chem.*, 2000, **43**, 3566–3572.
137 F. Mangiavacchi, L. Crociani, L. Sancineto, F. Marini and C. Santi, *Molecules*, 2020, **25**, 2711.
138 J. K. Vandavasi, W.-P. Hu, C.-Y. Chen and J.-J. Wang, *Tetrahedron*, 2011, **67**, 8895–8901.

139 C. M. Bernt, P. T. Burks, A. W. DeMartino, A. E. Pierri, E. S. Levy, D. F. Zigler and P. C. Ford, *J. Am. Chem. Soc.*, 2014, **136**, 2192–2195.
140 S.-J. Jeon, T.-W. Kang, J.-M. Ju, M.-J. Kim, J. H. Park, F. Raza, J. Han, H.-R. Lee and J.-H. Kim, *Adv. Funct. Mater.*, 2016, **26**, 8211–8219.
141 C. Han, Y.-H. Li, J.-Y. Li, M.-Y. Qi, Z.-R. Tang and Y.-J. Xu, *Angew. Chem., Int. Ed.*, 2021, **60**, 7962–7970.
142 X.-B. Li, Z.-J. Li, Y.-J. Gao, Q.-Y. Meng, S. Yu, R. G. Weiss, C.-H. Tung and L.-Z. Wu, *Angew. Chem., Int. Ed.*, 2014, **53**, 2085–2089.
143 R. Ray, A. S. Hazari, G. K. Lahiri and D. Maiti, *Chem.–Asian J.*, 2018, **13**, 2138–2148.
144 Y. Xu, Y. Chen and W.-F. Fu, *Appl. Catal., B*, 2018, **236**, 176–183.
145 X. Wu, N. Luo, S. Xie, H. Zhang, Q. Zhang, F. Wang and Y. Wang, *Chem. Soc. Rev.*, 2020, **49**, 6198–6223.
146 J. Ye, K. Ni, J. Liu, G. Chen, M. Ikram and Y. Zhu, *ChemCatChem*, 2018, **10**, 259–265.
147 X. Tu, Q. Wang, F. Zhang, F. Lan, H. Liu and R. Li, *Nanoscale*, 2020, **12**, 4410–4417.
148 D. W. Wakerley, M. F. Kuehnel, K. L. Orchard, K. H. Ly, T. E. Rosser and E. Reisner, *Nat. Energy*, 2017, **2**, 17021.
149 C.-H. Zhou, X. Xia, C.-X. Lin, D.-S. Tong and J. Beltramini, *Chem. Soc. Rev.*, 2011, **40**, 5588–5617.
150 X. Wu, X. Fan, S. Xie, J. Lin, J. Cheng, Q. Zhang, L. Chen and Y. Wang, *Nat. Catal.*, 2018, **1**, 772–780.
151 A. J. Ragauskas, G. T. Beckham, M. J. Biddy, R. Chandra, F. Chen, M. F. Davis, B. H. Davison, R. A. Dixon, P. Gilna, M. Keller, P. Langan, A. K. Naskar, J. N. Saddler, T. J. Tschaplinski, G. A. Tuskan and C. E. Wyman, *Science*, 2014, **344**, 1246843.
152 X. Wu, S. Xie, H. Zhang, Q. Zhang, B. F. Sels and Y. Wang, *Adv. Mater.*, 2021, **33**, 2007129.
153 S.-H. Li, S. Liu, J. C. Colmenares and Y.-J. Xu, *Green Chem.*, 2016, **18**, 594–607.
154 J. D. Nguyen, B. S. Matsuura and C. R. J. Stephenson, *J. Am. Chem. Soc.*, 2014, **136**, 1218–1221.
155 N. Luo, M. Wang, H. Li, J. Zhang, H. Liu and F. Wang, *ACS Catal.*, 2016, **6**, 7716–7721.
156 N. Luo, M. Wang, H. Li, J. Zhang, T. Hou, H. Chen, X. Zhang, J. Lu and F. Wang, *ACS Catal.*, 2017, **7**, 4571–4580.
157 I. Bosque, G. Magallanes, M. Rigoulet, M. D. Kärkäs and C. R. J. Stephenson, *ACS Cent. Sci.*, 2017, **3**, 621–628.
158 I. F. Teixeira, B. T. W. Lo, P. Kostetskyy, M. Stamatakis, L. Ye, C. C. Tang, G. Mpourmpakis and S. C. E. Tsang, *Angew. Chem., Int. Ed.*, 2016, **55**, 13061–13066.
159 N. Luo, T. Montini, J. Zhang, P. Fornasiero, E. Fonda, T. Hou, W. Nie, J. Lu, J. Liu, M. Heggen, L. Lin, C. Ma, M. Wang, F. Fan, S. Jin and F. Wang, *Nat. Energy*, 2019, **4**, 575–584.
160 Y.-H. Li, F. Zhang, Y. Chen, J.-Y. Li and Y.-J. Xu, *Green Chem.*, 2020, **22**, 163–169.
161 J. Qiao, Z.-Q. Song, C. Huang, R.-N. Ci, Z. Liu, B. Chen, C.-H. Tung and L.-Z. Wu, *Angew. Chem., Int. Ed.*, 2021, **60**, 27201–27205.
162 Z.-K. Xin, M.-Y. Huang, Y. Wang, Y.-J. Gao, Q. Guo, X.-B. Li, C.-H. Tung and L.-Z. Wu, *Angew. Chem., Int. Ed.*, 2022, **61**, e202207222.

